ESTIMATION OF SURROGATE RESPIRATION AND DETECTION OF SLEEP APNEA EVENTS FROM DYNAMC DATA MINING OF MULTIPLE CARDIORESPIRATORY SENSORS

By

KUNAL KARANDIKAR

Bachelor of Engineering in Electronics Engineering

University of Pune

Pune, India

2009

Submitted to the Faculty of the
Graduate College of the
Oklahoma State University
in partial fulfillment of
the requirements for
the Degree of
MASTER OF SCIENCE
July, 2012

ESTIMATION OF SURROGATE RESPIRATION AND DETECTION OF SLEEP APNEA EVENTS FROM DYNAMC DATA MINING OF MULTIPLE CARDIORESPIRATORY SENSORS

Thesis Approved:

Dr. Satish Bukkapatnam

Thesis Adviser

Dr. Bruce Benjamin

Dr. James Kong

Dr. Balabhaskar Balasundaram

Dr. Sheryl A. Tucker

Dean of the Graduate College

TABLE OF CONTENTS

LIST OF TABLES

Tables Page

LIST OF FIGURES

Figures Page

Figures Page

GLOSSARY OF TERMINOLOGY

1. ECG : Electrocardiogram
2. EMD: Empirical Mode Decomposition
3. RSA: Respiratory Sinus Arrhythmia
4. VCG: Vector cardiogram
5. DDM: Dynamic Data Mining
6. HSR: Heart Sound Derived Respiration
7. EDR: ECG derived Respiration
8. RS: Respiration derived from heart sounds (HSR)
9. EMD- HS: Respiration derived after implementing EMD on heart sounds
10. IMF: Intrinsic mode function
11. Breaths per minute (BPM)
12. Heart Rate Variability(HRV)
13. Recurrence Plot(RP)
14. Recurrence Quantification Analysis(RQA)
15. Principal Component Analysis (PCA)
16. Apnea hypopnea index (AHI)
17. Sleep Apnea/Hypopnea Syndrome (SAHS)

CHAPTER I

INTRODUCTION

Respiration studies have assumed increased importance in the field of biomedical analytics research. Respiration signal analysis is beginning to be applied to address a variety of issues ranging from cardiac diagnostics [18] and sleep studies [17], to sports medicine [19]. With the recent thrust towards wearable systems [67-69], and healthcare cost reduction, some research investigations have addressed the extraction of respiration waveforms from ECG data so that the number of sensors and total examination cycle times can be reduced [7, 8].

The basic principle underlying the derivation of respiration signals from an ECG is that respiration induces a modulation of the cardiac signal's electrical axis [1]. During inspiration, as lungs are gradually filled, the apex of the heart is stretched towards the abdomen. During expiration, the diaphragm is elevated, as it helps the emptying of the lungs. This action compresses the apex of the heart toward the breast. ECG analysis has therefore been a key tool in understanding respiration-induced heart displacement [2]. Respiration-induced changes in the ECG also make it possible to derive a surrogate respiratory signal directly from the ECG, potentially eliminating the need for a separate respiratory sensing system [3]. Different methods like empirical mode decomposition (EMD) [2, 8, and 10], heart rate variability [8] and wavelets [30-34]

have been used to derive respiration signals. While respiratory rates (i.e., the lengths of intervals between successive inspirations) extracted from the derived signals correlate well (correlation coefficient $\rho > 80\%$) with those extracted from the measured respiration signals [2], the respiratory waveforms derived from an ECG typically have $\rho < 40\%$.

In addition to ECG data, heart sounds serve as an important parameter to understand valuable information about the functional integrity of the heart. Heart sounds are the elastic waves emitted by the heart during a cardiac cycle [6]. Assessing heart sounds has almost always been a chief part of auscultation-based diagnosis at hospitals. Apart from being a low-cost alternative to the ECG, it is useful for detecting defects such as structural abnormalities in the heart and defects characterized by heart murmurs and abnormal sounds that cannot be detected using the ECG [4].

The timing and relative intensities of heart sound waveforms can be recorded using a digital stethoscope, and its graphic representation is called a phonocardiogram [39]. Unlike an ECG, current understanding of the heart sounds is still limited due to the nonstationarity (time varying nature) of heart sound dynamics, as well as the complexity and sheer diversity of the PCG signal patterns [4]. Since these are acoustic signals, they are prone to interference from several ambient noise sources that are difficult to isolate, even in well-controlled clinical or hospital environments [5]. These noises can be both internal (e.g., coughing and physiological variations) as well external (e.g., environmental noise). Pertinently, respiration is a prominent extraneous component that often affects proper diagnosis using heart sounds. Recent developments in digital signal analysis techniques can be used to better analyze heart sound signals and derive meaningful information from these components [4].

This research reports an approach to deriving respiration components from the measured heart sound signals. The data required for analysis was collected synchronously using a new wireless sensor unit (see Fig.1) built in the Sensor Networks and Complex Systems Monitoring laboratory (COMMSENS) at Oklahoma State University and a wearable sensor vest (see Fig. 2) from Vivo Metrics. The synchronous acquisition of heart sound and ECG data is a unique feature of our system and lays the foundation for the analysis that follows. The respiratory waveform derived from heart sounds (HSR) was compared with these two alternative methods, for, deriving respiration data from the ECG. The results show that the waveform as well as internal characteristics of the HSR correlate well with the measured respiration signal compared to other alternatives. The remainder of this document is organized as follows: Chapter 2 presents a brief review of methods reported in literature to extract respiration from an ECG and heart sounds, Chapter 3 presents the problem statement and research objectives, Chapter 4 presents our approach to deriving respiration from heart sounds and an ECG, and Chapter 5 describes validation studies and presents the results.

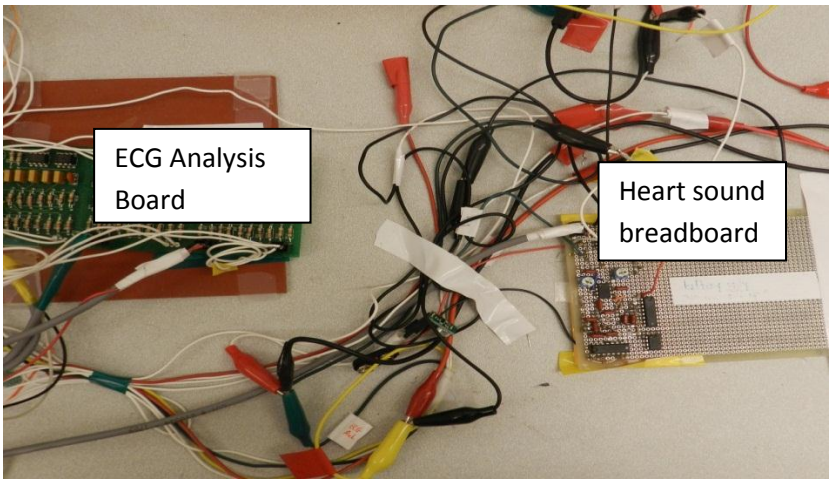

Figure 1: Wireless sensor unit setup in the COMMSENS laboratory at Oklahoma State University

Figure 2: Wearable sensor vest from Vivo Metrics.

CHAPTER II

BACKGROUND AND REVIEW OF METHODS TO DERIVE RESPIRATION SIGNALS

This chapter presents an overview of previous attempts conducted by several research groups to derive surrogate respiration. These attempts focus mainly on ECG derived respiration (EDR) methods. There has been a mention of deriving respiration from lung and body sounds which could provide alternatives in deriving surrogate respiration.

2.1 ECG DERIVED RESPIRATION (EDR) SIGNALS

Womack [20] was one of the early pioneers in deriving surrogate respiratory rate from ECG signals. Subsequently, several other techniques for deriving respiration from an ECG were developed. The early EDR techniques could be classified into four categories [21]. The first category is based on estimating ECG-derived respiratory (EDR) signals using heart beat interval fluctuations, also referred to as respiratory sinus arrhythmia (RSA) [20]. The second category, the "amplitude method" is based on the fact that the impedance across the thoracic cavity changes during inspiration and expiration so that the amplitude of the ECG's QRS complex changes [22-24]. Specifically, the EDR could be determined from the change in R-wave amplitude from the suitable lead ECG. The third category called the "area method" derives the EDR from the ratio of the area under the QRS complex in multiple lead ECG [25, 26]. The fourth, the angle of mean electrical axis (AMEA) method [27], estimates the EDR by finding the area of the QRS complex from any two lead ECGs, and then obtaining the AMEA from the arctangent of the ratio of

these areas. Leanderson [31] proposed a method based on the alignment of an observed vectorcardiogram (VCG) loop to a reference loop with respect to the transformations of rotation and time synchronization. Mazzanti et al. [32] proposed the method to automatically select the optimal leads to calculate the EDR from QRS-area validations. Bailon et al. [33] claimed that the conventional methods fail during stress testing since the ECGs contain highly nonstationary noise and rapid changes in the QRS complex. Also, they presented an area-based method that exploits the oscillatory pattern of the rotation angles of the heart's electrical axis induced by the respiration to derive the EDR. Based on the R-wave amplitude method, Ding et al. [24] calculated the kurtosis of intervals between each pair of neighboring R peaks instead of using the amplitude of the R-wave directly for deriving the EDR. Arunachalam et al. [34] presented a real-time algorithm for estimation and removal of baseline wander (BW) noise and then obtained the EDR by the amplitude method.

To address the limitations of conventional EDR methods in the presence of noise, Langley [29] proposed an algorithm based on principal component analysis (PCA) to derive the EDR from multiple lead ECGs. However, the PCA based EDR assumes that the respiration signals emerge from a linear process. Widjaja et al. [30] proposed a method that uses kernel PCA for nonlinear decomposition of ECG signals to derive respiration. Multiple groups have investigated empirical mode decomposition (EMD) for EDR [2, 8]. These studies indicate that EDR obtained from EMD has the highest correlation with the real respiratory signal compared to results obtained from other methods [8].

2.2 HEART SOUND DERIVED RESPIRATION (HSR)

Apart from the ECG, heart sound signals are widely collected during medical examinations, especially as a part of auscultation. Extraction of respiration from these signals, although plausible, has not received much attention. In this study we develop a new method to use heart sound signals gathered contemporaneously with an ECG to extract respiration and compare the resulting signals from EDR obtained using an ECG.

A heart sound waveform within a cardiac cycle is marked by multiple events (also referred to as waves), such as S1, S2, S3, S4 and heart murmurs (see Fig. 3). The heart sound waves occur over frequencies in the range of 10 Hz-2 KHz. The S1 sounds typically occur near in the 15-30 Hz frequency, while S2 sounds lie at or around 30-45 Hz as shown in Figure 4. Most heart sounds are generated by the closing and opening of semilunar and AV valves and associated flow phenomena [6]. Four classes of sound components, viz., S1, S2, S3 and S4 may be audible in a typical heart auscultation as shown in Figure 3. The prominent waves, S1 and S2 are always audible in a normal patient. The others, including S3, S4, clicks, snaps, and organic murmurs (as opposed to ‘‘innocent’’ murmurs), are present only under abnormal circumstances and in disorders [4]. Component S1 relates to the closing of the mitral and tricuspid valves while S2 is generated by the halting of the aortic and pulmonary valve leaflets [52]. Therefore, S1 happens almost contemporaneously with the QRS complex in an ECG (electrocardiogram) and S2 follows the systolic pause, which happens towards the end of the T wave in the ECG in a normal cardiac cycle. Therefore, heart sound events can be identified by correlating them with the corresponding ECG/cardiac events.

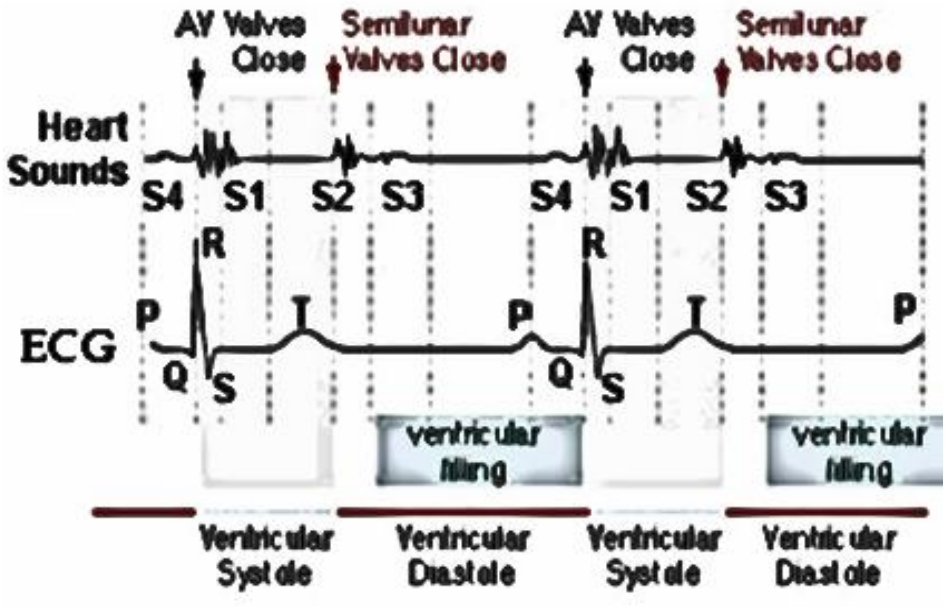

Figure 3: Schematic plot showing the timing of various EKG and heart sound events in two consecutive cardiac cycles [52]. The morphology of the prominent heart sounds S1, S2, S3 and S4 and the respective timings in the heart sound signal with respect to the ECG are provided.

Fig. 3 is a representative figure showing different classes of heart sounds and their respective timing with respect to the ECG signal. The figure also shows the timing of the ventricular pauses (systole and diastole) with respect to the ECG signal and the heart sounds. The systole begins at the end of S1 and lasts until the start of S2. The diastole on the other hand, relates to the ventricular filling, and begins at the end of S2 and lasts until the start of S1.

Fig. 4 shows the frequency information related to a heart sound signal of a supine subject recorded at 250 Hz. The horizontal axis contains the frequency information represented in Hz while the vertical axis contains the amplitude information relative to each frequency. The S1 component of heart sounds occurs within a frequency band of 15- 30

Hz while the S2 component of heart sounds occurs within a frequency band of 30-45 Hz, as indicated by the three dominant frequency modes in these bands.

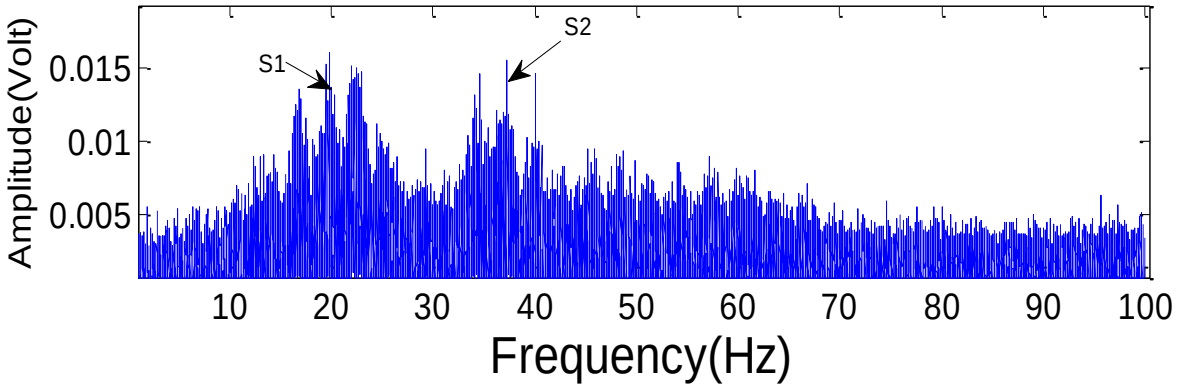

Figure 4: Frequency portrait of heart sounds. The horizontal axis represents the frequency in Hz while the vertical axis represents the amplitude(volt) relative to the frequency in volts. This heart sound signal was recorded from a supine subject at 250 Hz sampling rate .Heart sound signal S1 occurs near 20 Hz while S2 occurs near 35 Hz

Apart from heart sounds, body sounds emanate from various mechanical activities of the body organs. While the cardiac sounds can be measured around the heart or arteries, the respiratory sounds can be measured around the respiratory tract or lungs. Similarly, breath sounds can be measured at the trachea.

Miwa et al. [41] measured body sounds at the neck around the carotid artery along with an ECG and respiratory signals obtained from airflow sensors. Continuous Wavelet Transform [34] was applied to the body sound data, and the heart rate and respiratory rate were determined. The heart rate and respiratory rate, expressed in terms of breaths/min or bpm calculated from body-sounds, were reported to be near the 63 [bpm] and 10.1[bpm], ranges respectively. The heart rate and respiratory rate calculated from the ECG and

original respiratory waveform were also found to be near 63 [bpm] and 10.1[bpm]. Similarly, inter-beat intervals were coincident with the respiratory rate intervals (RRI) determined by the ECG. Some other groups have also attempted to use body sounds auscultation to gain information regarding breathing disorders [50, 51].

Typically, healthcare professionals use standard stethoscopes to measure respiration rate. But this technique is more prone to human errors. Another technique called phonopneumography, is used to more accurately count respiration rate [42-44]. Acoustic sensors using a microphone detect analog breath sound signals which can be digitized and analyzed using computer algorithms to monitor respiration rate. Respiration signals can also be derived by having an acoustic sensor carrying a microphone placed on the trachea. Some groups have proposed use of bioacoustics sensors to obtain respiration signals. [47-49]. Inspiration and expiration signals can be obtained by segmenting the acquired data into different frequency ranges which contain respiration and other cardiological data.

Noma et al. [45] proposed a method to obtain surrogate respiration using non-audible murmur (NAM) microphones. A NAM microphone was attached at the subject's neck. ECG data and heart sounds (phonocardiograms) were also obtained simultaneously along with respiratory information. Respiration information was reported to be contained in the 150-200Hz bandwidth in the acquired data. While NAM and trachea based estimates of respiration were found to be promising, they need an extra sensor, and these signals tend to be highly sensitive to body movement. However, the previous work does not report extensive validation of the surrogate respiration signals extracted and the experiments have not been tested under different conditions and on multiple subjects.

CHAPTER III

PROBLEM DESCRIPTION AND RESEARCH OBJECTIVES

Prior respiration studies have focused heavily on deriving surrogate respiration waveforms from ECG signals. The basic rationale behind the derivation of respiration from ECG is that respiration induces a modulation of cardiac signal's electrical axis [1]. As discussed before, many algorithms like Empirical Mode Decomposition (EMD), principal component analysis (PCA) and wavelets have been implemented with varying effects to extract surrogate respiration waveforms from ECG data [2, 29, 24]. Heart sounds, on other hand, also provide useful information pertaining to the cardiovascular dynamics of the heart. The human race was aware of the existence of these cardiac sounds as early as 460 B.C. [40], But they have been employed for cardiac auscultation only since Rene' Theophile' invented the stethoscope in the 17^{th} century [40]. Heart sounds even today remain the primary source of auscultation at hospitals. However, extracting respiration information from these cardiac sounds has received little attention.

This study addresses the need to study heart sounds as a possible alternative to traditional ECG derived respiration information. We have investigated a new method to estimate heart sounds based on ensemble averaging, as detailed in Chapter 4.1. To validate our algorithm, we have compared the waveform characteristics obtained using heart sounds with traditional ECG-derived respiration techniques as well as with the real-time respiration measuring instrument from Vivo Metrics. Specifically, we compare the

signals based on how well the respiration waveform, the peak to peak intervals, RSA and zero crossing intervals of the derived signals compare with those from the measured respiration signals (see Chapter 5). There are two perceivable benefits of conducting this study as listed below:

1. Economic savings: As heart sounds are easily accessible to the doctor, there will be significant cost savings in terms of reduced technology (sensors and accessories) required to estimate respiration as compared to traditional heart sound derived respiration
2. Ergonomic value: Reducing/eliminating the number of sensors required will make the process of collecting data much easier for the doctor and painless for the subject.

We believe that heart sound analysis should be treated in more detail in order to generate other meaningful information related to cardiology such as structural abnormalities in the heart and defects characterized by heart murmurs. Also, there remains the possibility of calculating the respiratory rate measured using heart sounds and finding patterns to predict disorders like sleep apnea. This research has attempted to address some of these issues and we believe the results could lead us to some important insights pertaining to cardiovascular dynamics and diagnostics.

CHAPTER IV

RESEARCH METHODOLOGY

An overview of the procedure to extract respiratory waveforms from human subjects from ECG signals and heart sound data recorded simultaneously and synchronously using our new wireless sensor technology is presented in Fig. 5. The wearable vest from Vivo Metrics that records a single channel ECG and respiratory signals is used for validation studies of the desired respiration signals.

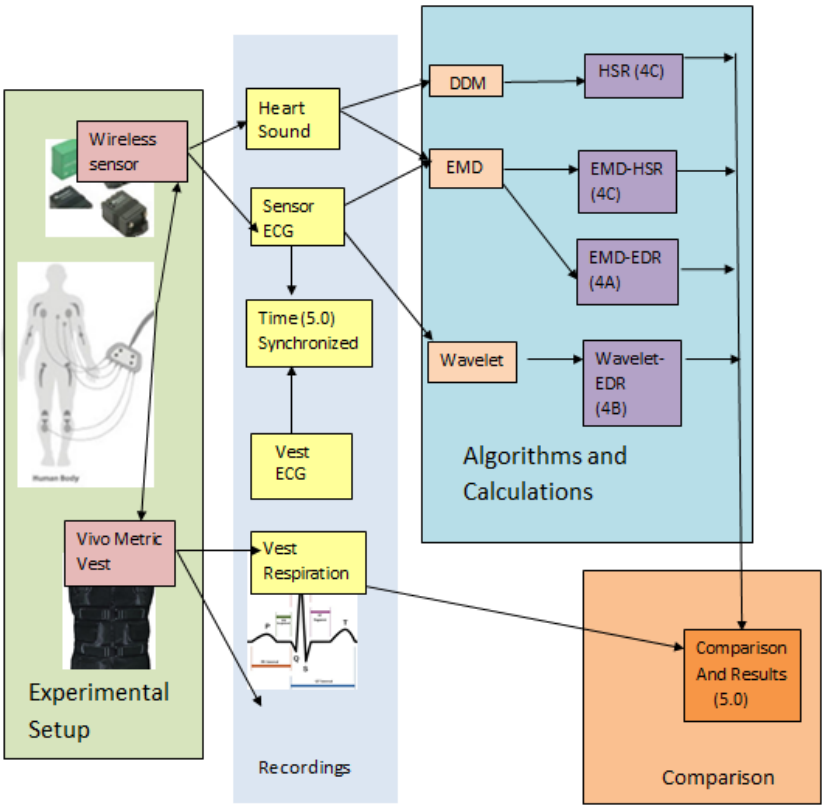

Figure 5: Overview of surrogate respiration extraction methods

All experiments were carried out in the Sensor Networks and Complex Systems research laboratory (COMMSENS) at Oklahoma State University on 20 healthy male subjects with an age range of 25-35 years. The subjects were instrumented with two sensor suites, namely, a wireless unit developed at the COMMSENS lab and a wearable vest obtained from VivoMetrics. The samples were collected for a duration of ten minutes each. The sensor unit consisted of an electronic circuit connected to the electrodes, as well as a Bluetooth wireless unit to transmit Frank's XYZ signals and one channel for transferring heart sound data to a remote computer for storage and analysis. The sensor unit uses 8 electrodes- two each for X, Y, and Z axes, one for the heart sound and one for ground. The wireless sensor data was sampled at 250 Hz, and the single channel ECG and two channels of respiration signals (abdomen and ribcage) from the Vivo Metrics vest were sampled at 200 Hz. The data were collected from ten healthy subjects under 2 different physical states: upright standing (see Fig. 6), and supine (see Fig. 7).

Figure 6: Male subject in an upright standing posture. The samples were collected at the rate of 250 Hz using the wireless sensing unit while the vest collected samples at the rate of 200 Hz.

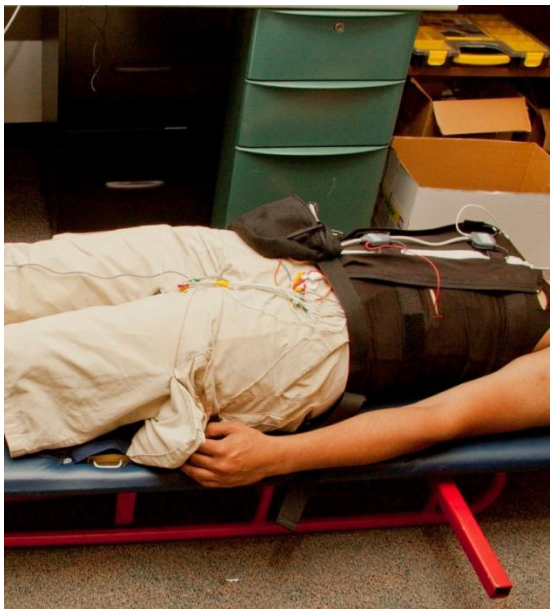

Figure 7: Male subject in a supine posture. The samples were collected at the rate of 250 Hz using the wireless sensing unit while the vest collected samples at the rate of 200 Hz.

There is a marked reduction in the number of electrodes (7 vs. 15) in the wireless unit as compared to the traditional 12-lead method. However, no discrepancies were found in the data collected. The ECG signals from the wireless system are time-synchronized with those from the vest to allow comparison of corresponding ECG and respiration waveforms from the vest and the wireless unit. The method for extracting surrogate respiration waveforms from heart sounds is based on identifying the salient heart sound signal patterns with the help of easily identifiable events from synchronously acquired ECG signals. Here, a nonlinear time scaling is applied on the measured heart sound signals to obtain an ensemble of time- averaged waveforms [12]. The scaling method relies on treating the signal as a cyclostationary process [53]. The respiration component is treated as the difference between the measured and averaged signals. Chapter 4.1 describes this method of deriving respiration from heart sounds using a time averaging

method where, non-linear time scaling is applied to obtain an ensemble average signal, which facilitates the estimation of a respiration waveform. The resulting signal is compared with respiration signals measured concurrently from the Vivo Metrics vest, as well as EDR signals obtained using EMD and wavelet methods . In the EMD method described in Chapter 4.2, ECG data is processed into intrinsic modes of oscillation having equal number of extrema and zero crossing. Chapter 4.3 describes another method to estimate respiration using wavelet theory. Chapter 4.4 compares the performance of surrogate respiration obtained from heart sounds using EMD with the respiration obtained using the ensemble averaging method. A brief description of these methods is presented in the following subsections.

4.1 HEART SOUND DERIVED RESPIRATION

As mentioned above, our wireless sensing unit collects heart sounds synchronously with ECG data. This unique feature allows us to extract heart sound events efficiently through mapping with the ECG patterns, as well as to compare performances of alternative methods for extracting surrogate respiration signals. The measured heart sound signal can be written as

$$y(t) = x(t) + v(t) \quad (1)$$

where, $y(t)$ is the measured heart sound signal, $x(t)$ is the noise-free heart sound waveform i.e., ideal signal, and $v(t)$ is noise. Here, $x(t)$ is assumed to be cyclostationary [12], i.e.,

$$x(t) = x(t + nT), \quad (2)$$

and $v(t)$ is assumed to be a superposition of respiration and other ambient noise processes which are zero mean and independent of each other and $x(t)$, i.e.,

$$v(t) = v_l(t) + v_c(t) \quad (3)$$

where, $v_l(t)$ is a low frequency component of $v(t)$ that connotes respiration, and $v_c(t)$ is the complementary noise component that emerges from all other sources. Since $y(t)$ is cyclostationary, the noise-free signal component $x(t)$, can be estimated by averaging over all the cycles of the signal. Since different signals have different periods, one needs to take a time-scaled ensemble average of the signal [12]. According to the central limit theorem, the average of the large number of independent random variables follows a normal distribution with the mean close to the true mean of the cyclostationary signal.

Fig. 8 summarizes the method used to estimate surrogate respiration from heart sounds.

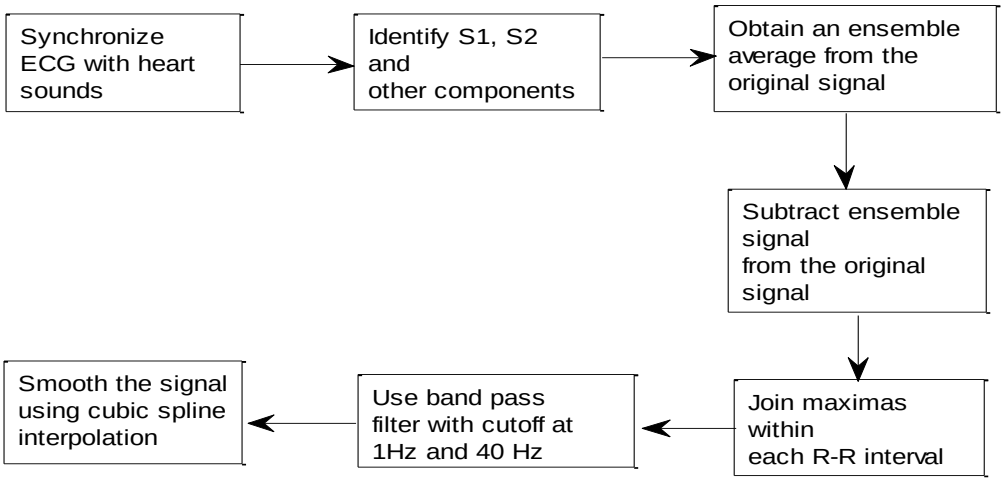

Figure 8: Steps involved in deriving surrogate respiration using the ensemble averaging technique.

The task has been made simpler due to unique feature of our system which performs synchronous measurement of ECG and heart sounds. This synchronous recording facilitates segmenting the heart sounds into different components which forms the basis for the further analysis. The following points describe the method to estimate respiration in greater detail.

Identify S1 and S2. The sound components S1 and S2 have similar and often statistically indistinguishable time and frequency patterns. It is therefore challenging to correctly identify S1 and S2 components of a heart sound signal automatically. Sound component S1 occurs due to the closing of mitral and tricuspid valves, and it is generally synchronous in time with the peak of the QRS wave. Also, S2 follows the systolic pause that begins at the end of the T wave in the ECG. Therefore, it is not hard to segment heart sounds S1 and S2, and the systolic and diastolic pauses within them when ECG data is employed as a reference. Hence, the synchronous measurement of heart sounds and ECG helps to identify S1 and S2 waves. Fig. 9 shows the alignment of heart sounds using ECG data as reference. The R peak in the QRS component of the ECG waveform, marks the beginning of the S1 component in the corresponding heart sound waveform measured synchronously. The end of the T wave in the ECG waveform, marks the beginning of the S2 component in the corresponding heart sound waveform. The samples were recorded from a healthy male subject in a supine position. The samples were collected at the sampling rate of 250 Hz.

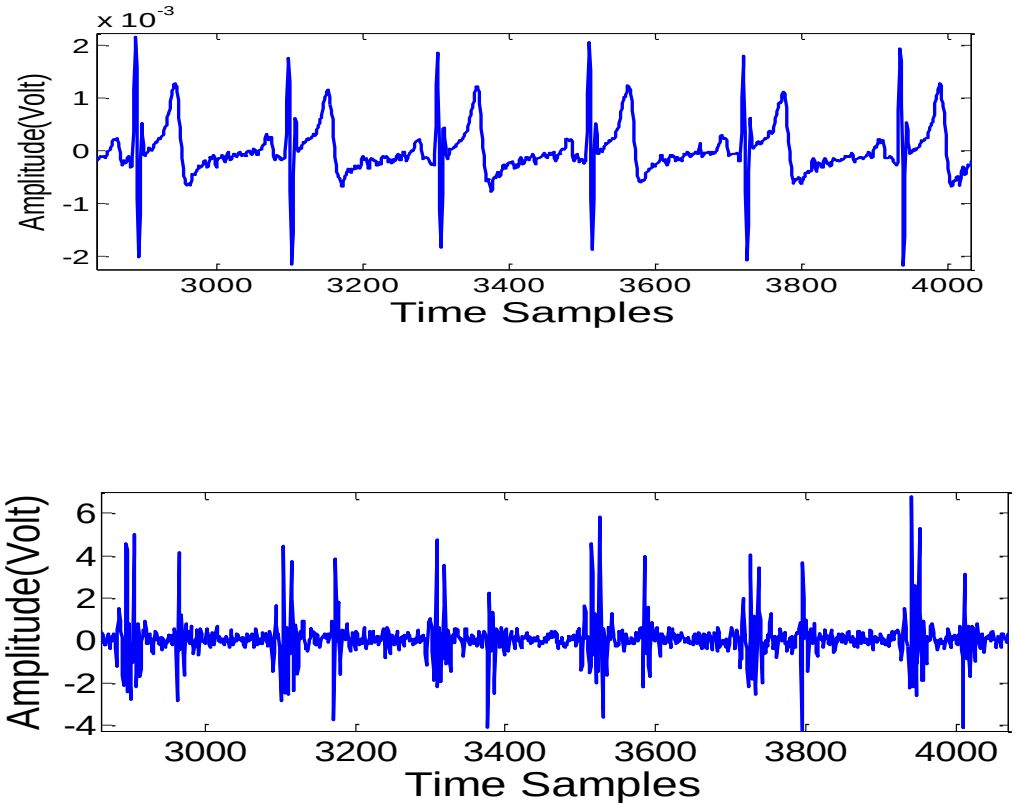

Figure 9: Synchronized ECG and heart sound. The horizontal axis consists of time represented in sample points while the vertical axis consists of amplitude(volt) measured in volts relative to the time samples. Here, the samples were collected at the rate of 200 Hz from a healthy supine subject.

Derive Ensemble Average. Heart sounds as shown in Fig. 10, are roughly cyclostationary in nature, i.e., $E[v_l(t).v(t+\tau)] = E[v_l(t).v(t+T+\tau)]$ for any time t, $\tau = I\mathbb{R}^+$, and T is the average beat length. The characteristics of S1 and S2 waveforms (as observed from overlaying on each other) varied little from beat-to-beat as shown in Fig. 10. According to Tang et al. [12], the average correlation between two S1 waves from different beats was 0.97, and that between S2 waves was 0.95. Heart cycle duration, however, varies from cycle to cycle [12]. This variation, generally known as heart rate variability (HRV) influences changes in cyclic stationarity. To account for this variability, we employ nonlinear time scaling on the signals. In nonlinear time scaling,

the timings of heart sounds are aligned from cycle to cycle, with the first heart sound cycle used as a reference. For every subsequent cycle in the heart sound signal, we keep the S1 and S2 samples of equal size and interpolate the systole and diastole samples (to align the timing of the cycles with the reference.) The nonlinear function used to perform nonlinear time scaling for the i^{th}cycle is defined as $f_i(a_i; t)$.where a_i is the parameter vector

From [12], the heart sound signals of the following cycles become:

$$h_i(t) = h_i(f_i(a_i;t)) \quad \text{for i>1} \tag{4}$$

Here, the first cycle $h_1(t)$ is the reference cycle. T_i is the cycle duration for the i^{th}cycle. Fig. 11 shows the piecewise nonlinear function to estimate the ideal heart sound cycle. Segments 2-4 and segments 7-10 on the horizontal-axis represent S1 and S2, respectively.

Hence the piecewise function is parallel with the reference cycle for these segments. We interpolate segments 1-2 and 4-7 (on the X-axis) which represent the diastole and systole, respectively in order to match them with the reference cycle. The interpolation is shown by the change in slope in the random cycle for segments 1-2 and 4-7. By constructing the interpolated signal using the $f_i(a_i; t)$ functions as mentioned in [12], we are able to generate a heart sound cycle which is equal over the entire signal. Here, $x(t)$ which is the ideal heart sound cycle can thus be written as,

$$x(t) = {}^{1}/_{L} \sum_{t=1}^{L} y(t) \tag{5}$$

Where, $y(t)$ is the cycle duration at time, $t \in [1, L]$ and L is the number of cycles involved in the ensemble.

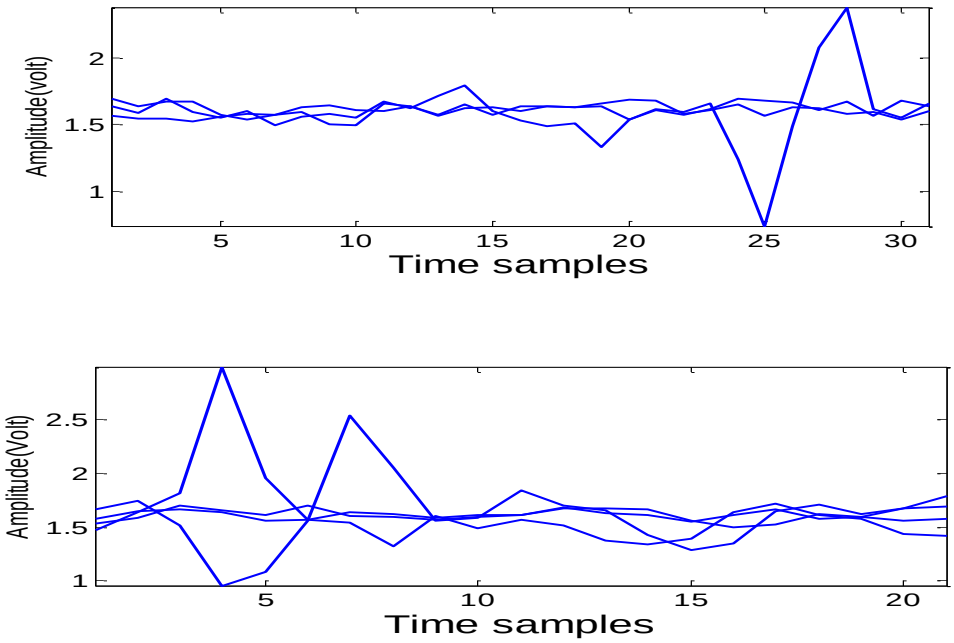

Figure 10: Cyclostationarity in heart sounds. S1 and S2 samples remain consistent from beat to beat. The horizontal axis shows time represented in sample points. The vertical axis shows the amplitude(volt) relative to each sample point represented in volts

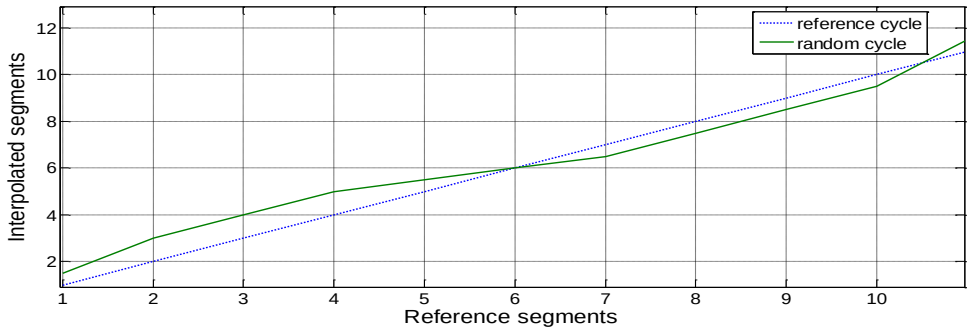

Figure 11: Piecewise function of nonlinear time scaling. The dotted line shows the cycle time of the reference cycle [1st cycle] while the solid line shows the interpolated cycle time of any random sample

This heart cycle in the resulting signal $x(t)$ comprises an ensemble average of each subcomponent of heart cycle, namely, S1, S2, systole and diastole joined together. This

heart cycle symbolizes the expected heart cycle of a virtual ideal heart. This heart cycle is replicated over the entirety of the signal. This obtained signal is shown in Fig. 13.

Subtract Ensemble Average. As this ensemble signal is the expected ideal heart sound signal, any aberrations with this signal are termed noise. As respiration forms a part of this noisy signal, extracting noise is of interest to us, i.e., if we subtract this signal from the original signal, we will be left with noise.

$$v(t) = y(t) - x(t) \tag{6}$$

This signal contains information regarding respiration $v_l(t)$ and external noise $v_c(t)$. We will have to further analyze this signal to obtain the surrogate respiration signal.

Separate Respiratory Component. Several algorithms in the literature [12] mention ways to extract noise from the heart sounds. Adaptive noise cancellation is successful in enhancing heart sounds, but an additional reference signal representing a version of the primary input signal with a weak or essentially undetectable information carrying component is required [13,14]. Also, reduced-order Kalman filter and spectral subtraction have been applied to remove noise from heart sounds [15, 16]. These methods may degrade if noise and disturbance are non-Gaussian, non-stationary, or colored. Robust methods for the noise reduction of heart sounds are therefore needed [22]. To extract noise from the heart sound data, from Eq (5) we subtract the ensemble signal from the original heart sound signal.

Figures 12-14, explain the signal processing on heart sound waveforms. Heart sound data recorded from a healthy subject in an upright posture is pictured in Fig. 12. The heart sound waveform consists predominantly consists of S1 and S2 components. S3, S4 and

other murmurs (if any) are not dominant. Fig. 13 is a pictorial representation of the ensemble heart sound data derived using Eq (4). The S1 and S2 components along with the systole and diastolic pauses, recorded over different beats, were added together and the mean of each phase was calculated. The averaged phases were then aggregated to represent them as one signal. Further, this averaged signal was repeated over the entirety of the signal. The ensemble signal waveform derived thus, is pictured in Fig. 13. Fig. 14 shows the residual signal extracted after subtracting the ensemble data from the original heart sound sample. The ensemble signal is assumed to be the heart sound signal of an ideal heart. Any aberrations to this signal are termed noise. Also, respiration is believed to form a part of the noise.

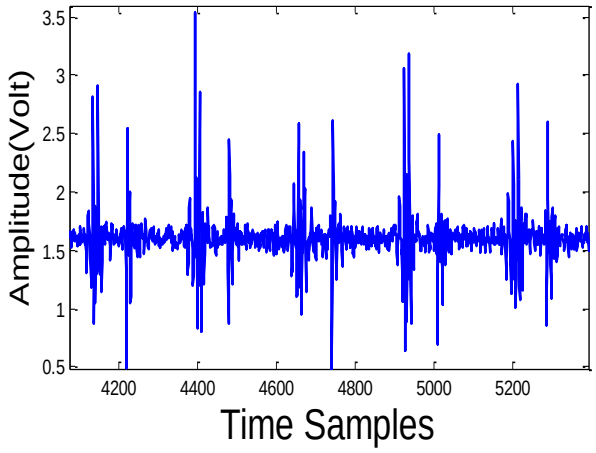

Figure 12: Heart sound data for an upright subject recorded at 250 Hz. The horizontal axis shows time represented in sample points. The vertical axis shows the amplitude(volt) relative to each sample point represented in volts

As respiration occurs due to the modulation in amplitudes, it can be derived by determining the extremas (maxima or minima) of the signal obtained in Eq. (6) (here the maxima in each heart cycle are obtained by writing a Matlab code). Once all the maximas

are obtained over the entirety of the signal, they are joined together. This obtained signal is band limited with cutoff frequencies at 1Hz and 40 Hz. This filtering helps eliminate artifacts due to baseline wandering. We also perform a cubic spline interpolation over this signal to get a better smoothing effect.

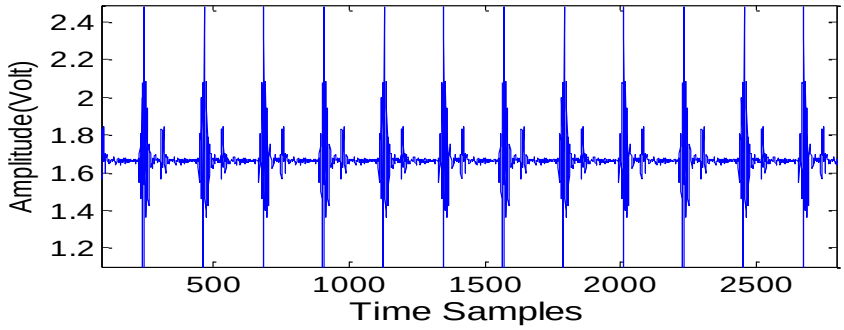

Figure 13: Ensemble averaged signal stretched across the entire signal length. The horizontal axis shows time represented in sample points. The vertical axis shows the amplitude (volt) relative to each sample point represented in volts

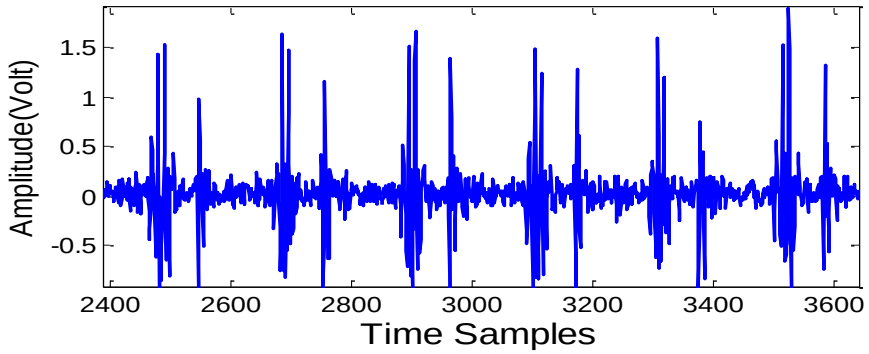

Figure 14: Noise obtained by subtracting the ensemble signal from the original signal. Here the samples were recorded at the rate of 250 Hz rate. The horizontal axis shows time represented in sample points. The vertical axis shows the amplitude(volt) relative to each sample point represented in volts

The resulting signal is treated as heart sound derived respiration, as shown in Fig. 15. The frequency representation of the heart sound derived respiration waveform is shown in Fig. 16. The horizontal axis represents the frequency in Hz while the vertical axis represents the amplitude (in volts) relative to the corresponding frequency. As is evident from the figure, a frequency peak exists near 0.3 Hz. Respiration is believed to be contained in a frequency range of 0.2-0.4Hz. The frequency peak's being at 0.3 Hz in this case, further validates the premise that the derived waveform contains a respiration component.

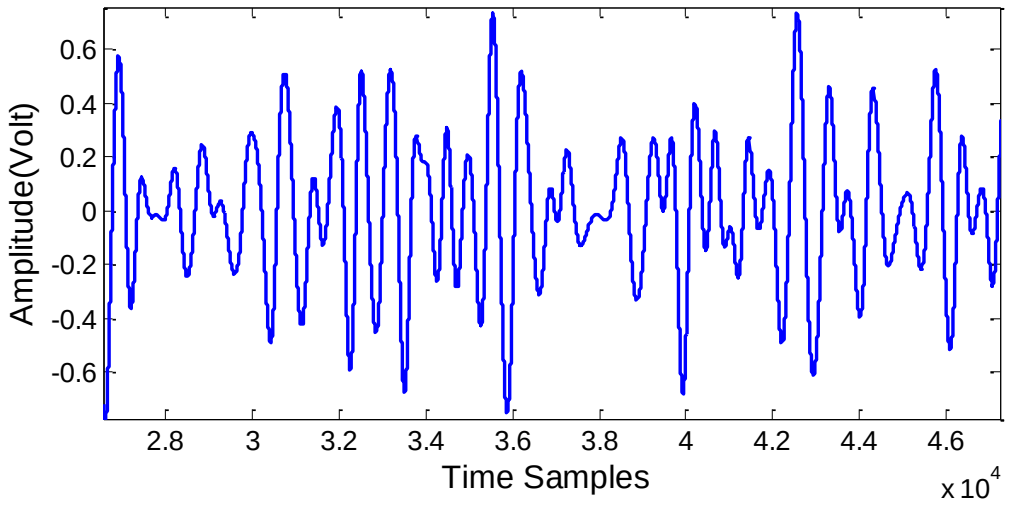

Figure 15: Heart sound derived respiration waveform. The horizontal axis shows time represented in sample points. The vertical axis shows the amplitude(volt) relative to each sample point represented in volts

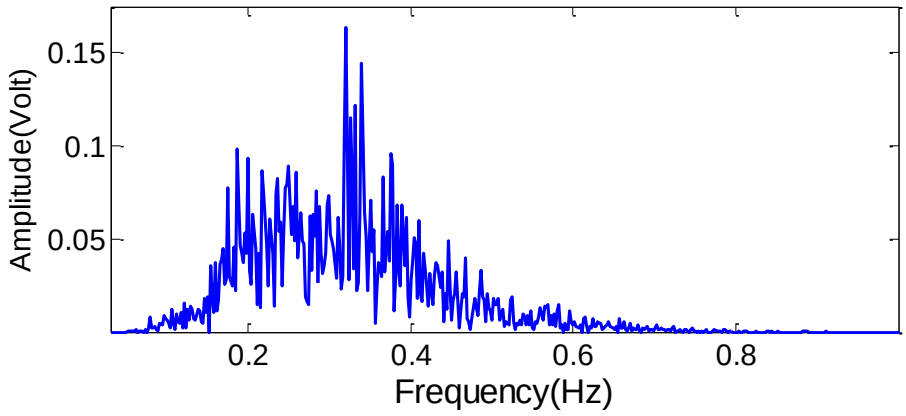

Figure 16: Frequency domain representation of heart sound derived respiration signal. The mode is obtained at 0.3 Hz and is believed to be the respiration component. The horizontal axis represents the frequency in Hz while the vertical axis represents the amplitude(volt) relative to a corresponding frequency in volts.

4.2 EMPIRICAL MODE DECOMPOSITION METHOD

The EMD method has met with notable success in the field of biomedical research, particularly in ECG analysis [9-11]. Empirical mode decomposition (EMD) is a method proposed by Huang et al. [7] that can be applied to study nonlinear and nonstationary properties of a time series. According to Campolo et al. [8], EMD performs better than other ECG derived respiration algorithms like the heart rate variability method and wavelet transform in terms of capturing the waveform and respiratory rate characteristics. The EMD method separates time-series into intrinsic oscillations using local, temporal and structural characteristics of the data [8]. The decomposition is done on the assumption that any data consists of different intrinsic modes of oscillation [7].

EMD is obtained through a process called sifting. It decomposes a signal into low and high frequency components called intrinsic mode functions (IMFs) [2]. Each intrinsic mode represents a simple oscillation having an equal number of extrema and zero crossings, i.e., the oscillations are symmetric w.r.t local mean. Also, the mean value of the envelope defined by local maxima and local minima is zero [2]. Another view of EMD involves treating a signal to be composed of a sum of low frequency components and a high frequency component. The high frequency part is called the intrinsic mode function (IMF) while the low frequency part is called the residual, i.e., the signals can be represented as

$$x(t) = \sum_{i=1}^{n} s_p(t) + r_{n+1}(t) \quad (7)$$

where, $h_i(t)$ are the IMF's and $r_n(t)$ is the residual. The basic procedure to extract the IMFs is stated in the following algorithm:

1. *Identify local extrema (maxima and minima)*
2. *Use a cubic spline interpolation to define upper and lower envelopes by connecting all maxima* e_{max} *and all minima* $e_{min}(t)$ *separately.*
3. *Calculate the local average at time ( ) .*

$$m(t) = (e_{min}(t) + e_{max}(t))/2 \quad (8)$$

4. *Compute the intrinsic mode functions (IMF's)* $s_p(t)$ *iteratively through a series of Reductions* $h_k(t) = r_{p-1}(t) - m_k(t)$, $k = 1, \ldots K_{max}$, $p = 1, \ldots, P$, $r_o(t) = x(t)$ (9)

Here, $h_k(t)$ *is treated as a series,*

$m_k(t)$ *is computed as the mean of upper and lower envelopes of* $h_k(t)$

5. *The process will repeat all steps until the following stoppage criterion (SD) is reached.*

$$= [\sum_{t=0}^{T} \left| h_{k-1}(t) - h_k(t) \right|^2] \; / \; [\sum_{t=0}^{T} h_{k-1}{}^2(t)] \; < \; SD \qquad (10)$$

6. *Obtain the residual* $r_p(t)$

$$r_p(t) = r_{p-1}(t) - s_p(t) \qquad (11)$$

We repeated this procedure on the residual obtained after each iteration until in the whole data set, the number of extrema and the number of zero crossings either are equal or differ at most by one; and finally, at any point, the mean value of the envelope defined by the local maxima and the envelope defined by the local minima is zero. On computing all the IMFs we finally sum the IMFs lying in the range of respiration (0.2-0.33Hz). This aggregate signal represents a surrogate respiration signal. Fig. 17 shows a representative EDR derived from an ECG signal of a healthy subject in a supine position using EMD.

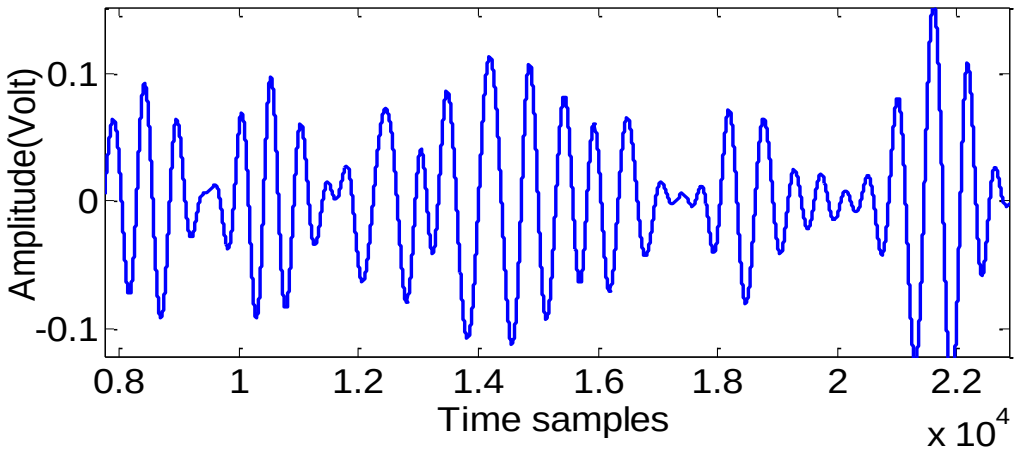

Figure 17: Surrogate respiration wave derived using EMD. The horizontal axis shows time represented in sample points. The vertical axis shows the amplitude(volt) relative to each sample point represented in volts

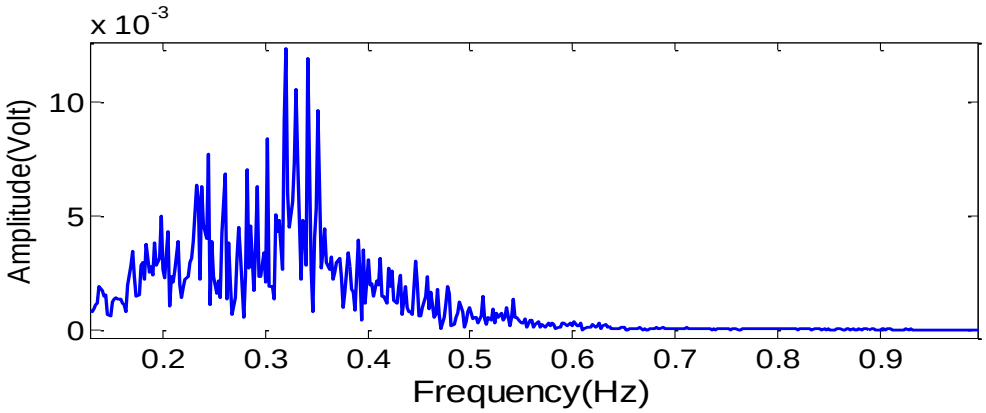

Figure 18: Representation of EDR derived using EMD in frequency domain. The mode can be seen at 0.3 Hz which represents the respiration component. The horizontal axis represents the frequency in Hz while the vertical axis represents the amplitude(volt) relative to a corresponding frequency in volts.

The waveform is a superimposition of IMFs lying in the range of normal respiration (0.2-0.33Hz). Fig. 18 shows the representative EDR waveform shown in Fig. 17 represented in the frequency domain. The frequency peak being at 0.3 Hz in this case, further validates the assumption that the derived waveform contains a respiration component.

4.3 WAVELET METHOD

In this method, we have derived the respiratory waveform from an ECG using the amplitude method which is based on changing the amplitude of the R-wave in the QRS complex.

The procedure employed is summarized as followed:

1) Filter the ECG from X-lead (Frank XYZ system) sampled at 200 Hz, using a 300th order FIR high pass digital filter in Matlab at the cutoff frequency of 1 Hz. This step will

eliminate the baseline wandering effect. It causes the baseline of the ECG signal to fluctuate from the normal position.

2) Use wavelets to find the time locations and amplitudes of R-peaks, and form a pulse train of R-peaks at their respective locations.

3) Use a cubic spline interpolation method to obtain a uniformly sampled pulse train, and treat the resulting signal as the surrogate for respiration information.

The result here is the EDR (ECG derived respiratory) signal. However, in a particular case when T-wave amplitudes are relatively high compared to the R-peak, most of the algorithms to detect the R-peak fail. They erroneously recognize the T-wave as the R-wave resulting in an inaccurate EDR signal. Fig. 19 shows one such instance. It is an ECG waveform recorded on a supine subject at a sampling rate of 250 Hz.

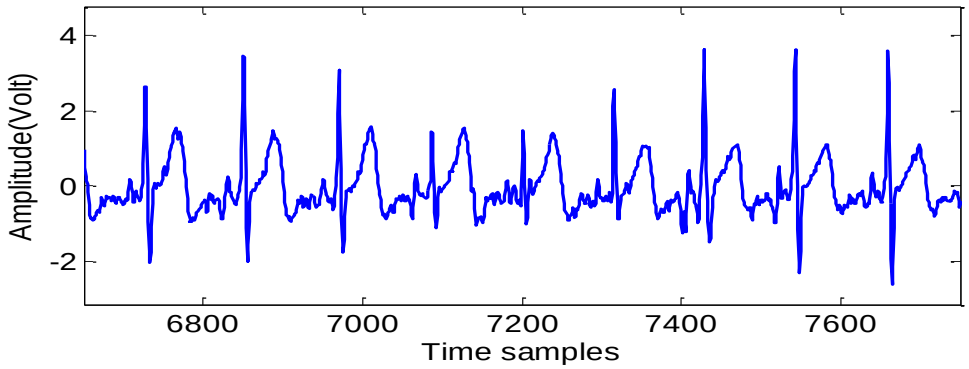

Figure 19: ECG signal with a high amplitude T-wave. Here the samples were extracted at 250 Hz rate. The horizontal axis shows the time represented in sample points. The vertical axis shows the amplitude(volt) relative to each sample point represented in volts .

To solve this problem, we propose a method to reduce the amplitude of the T-wave by using a wavelet decomposition method. Coiflet 5 is used for this purpose. The signal is decomposed at eight levels. Then, the decomposed signals only from levels 1-5 are used

for reconstruction. The reconstructed signal is shown in Fig. 20. Fig. 21 shows three waveforms, viz., the derived respiratory waveform (thick dashed line), rib cage respiration waveform (solid line) and abdominal respiration waveform (thin dashed line).

The abdominal and rib cage respiratory waveforms appear in phase and have similar frequency content. The derived respiration waveform appears slightly out of phase as compared to the other signals but appears to have similar frequency distribution.

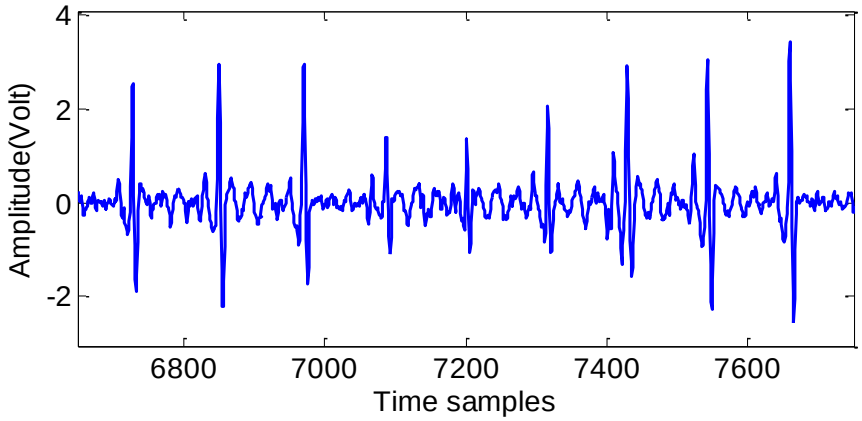

Figure 20: Reconstructed ECG signal from level one to five of wavelet decomposed signals. Here the samples were extracted at 250 Hz rate. The horizontal axis shows time represented in sample points. The vertical axis shows the amplitude(volt) relative to each sample point represented in volts

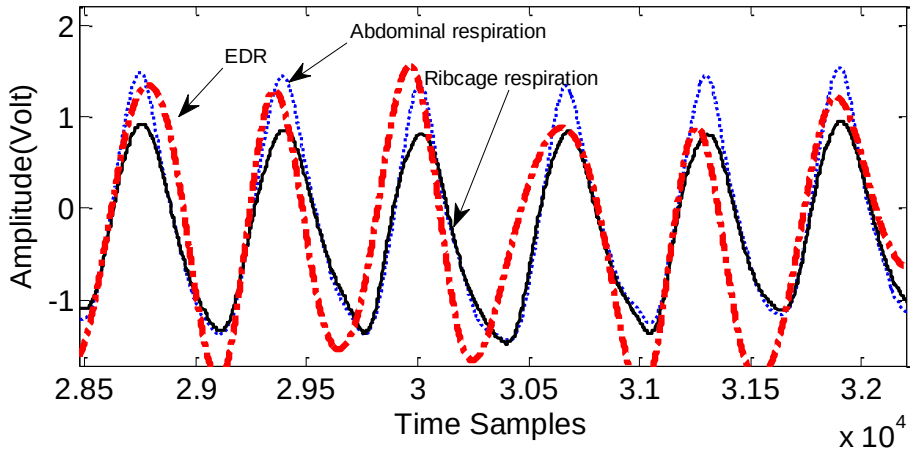

Figure 21: Signal Comparison between EDR signal (thick dashed line), Rib-cage respiratory (solid), and abdominal respiratory (thin dashed line). The horizontal axis shows time represented in sample points. The vertical axis shows the amplitude (volt) relative to each sample point represented in volts

4.4 HEART SOUND DERIVED RESPIRATION USING EMD

For validation purposes, we have also implemented EMD on heart sounds to compare surrogate respiration obtained using EMD with the surrogate respiration obtained using ensemble averaging as discussed in this section. The heart sound signal is decomposed into intrinsic mode functions similar to the ones obtained in Chapter 4.1. The intrinsic mode functions lying within the respiration frequency range (0.2 Hz-0.33 Hz) are added up to represent the surrogate respiration derived from heart sounds.

Fig. 22 shows the surrogate respiratory signal obtained after applying EMD on heart sounds. The figure shows the derived respiration waveform for a healthy subject in a supine state recorded at a sampling rate of 250 Hz. Fig. 23 shows the frequency domain representation of the obtained surrogate respiratory signal. The mode is obtained at 0.33

Hz and lies in the respiratory range. This range indicates that the derived surrogate respiration waveform may contain respiratory content.

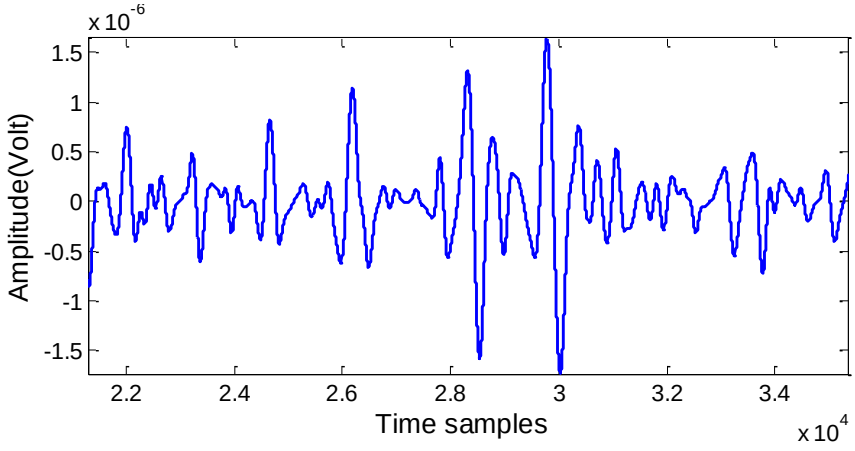

Figure 22: Surrogate respiration obtained applying EMD on heart sounds. The horizontal axis shows time represented in sample points. The vertical axis shows the amplitude(volt) relative to each sample point represented in volts

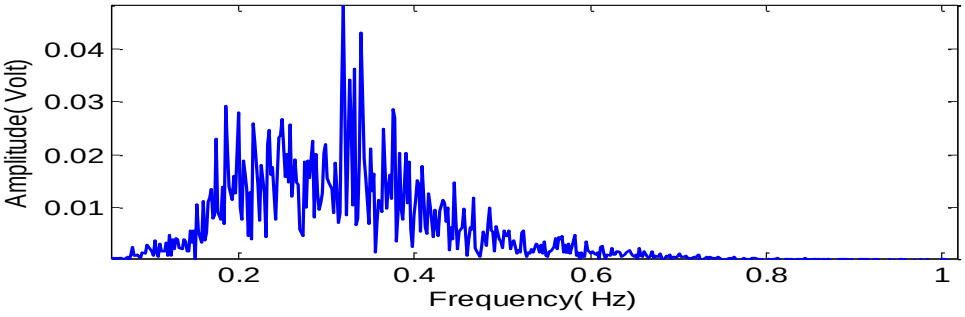

Figure 23: Frequency domain representation of heart sound derived respiration signal using EMD. The horizontal axis represents the frequency in Hz while the vertical axis represents the amplitude (volt) relative to a corresponding frequency in volts.

In summary, different methods to derive surrogate respiration from ECG and heart sounds have been discussed. The surrogate respiration obtained using these methods, was compared and the comparison summary has been documented in the Chapter 5.

CHAPTER V

VALIDATION STUDIES AND RESULTS

To validate the results, we compared our results with the real respiratory signal. Along with collecting the ECG and heart sound data from our sensor, we also collected ECG data and respiration data using Vivo Metric's respiration and ECG measurement device. The data collected using our sensor and the machine was synchronous with a lag in the range of 10-20 sec. The lag was mainly due to either delay in human measurement or the machine's internal processing boot up time. This lag was eliminated by synchronizing the ECG signals obtained by the machine and the sensor. Cross correlation was used to align the two ECG signals. Cross correlation is defined as a measure of similarity between two waveforms as a function of time lag applied to them. Its mathematical expression is as follows:

$$R_{XY}(t1, t2) = E[X(t1) * Y(t2)] \quad (12)$$

Upon alignment, the correlation between the two ECG signals was in the range of 99.1%-99.5%. Along with the ECG, the machine also synchronously measures respiration at the ribcage and at the abdomen. Surrogate respiration data obtained using EMD, wavelets and heart sound was compared with these measured signals using Pearson's correlation (See Table 1). Apart from wave to wave correlations, we have also calculated the correlation between the respiratory rate and frequency accuracy for the

four signals. The respiratory rate was calculated in 3 ways: 1.) using RSA functionality in AcqKnowledge 4.0 application. 2.) determining correlation between zero crossing intervals for all four signals, and 3.) calculating the correlation between peak to peak intervals for all signals and comparing them against peak to peak intervals of the measured respiration signal.

The measured and the derived respiration signals using heart sound and ECG are shown in an overlay portrait in Fig. 24. We observe that the wave to wave correlation of all signals w.r.t real respiration is rather low (ρ <60%). However, the frequency range of all derived respiration signals as well as the respiratory rate and the peak to peak intervals seems to match well with the real respiration (ρ >70%). This finding can also be validated by the results in the Table 1.

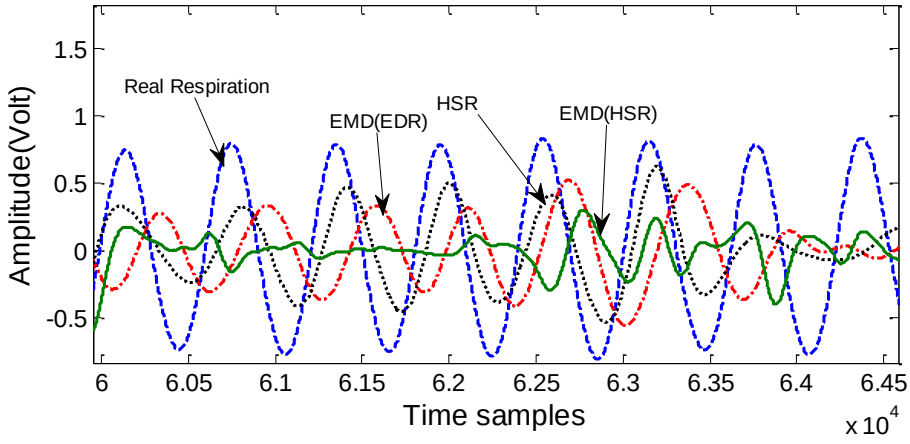

Figure 24: All four signals (Real respiration (measured from Vivo Metric's Vest, EMD derived surrogate respiration (EDR), heart sound derived surrogate respiration and EMD derived heart sound respiration) are plotted together.

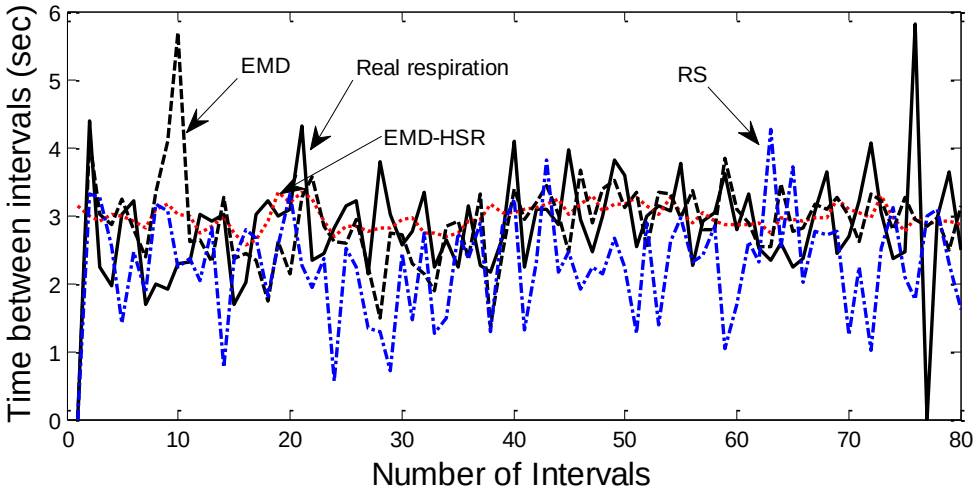

Figure 25: All four signals (Real respiration (measured from Vivo Metric's Vest, EMD derived surrogate respiration (EDR), heart sound derived surrogate respiration and EMD derived heart sound respiration) in terms of breathing intervals.

Fig. 25 depicts the four signals in terms of breathing intervals. The breathing intervals represent the peak to peak time and are expressed in seconds. The X axis displays the number of intervals over the sample signals, while the Y axis represents the breathing intervals in seconds. Here, RS refers to heart-sound-derived surrogate respiration, EMD to ECG-derived surrogate respiration obtained using the EMD method, EMD-HSR to the surrogate respiration obtained using the EMD method on heart sounds, and WDR-to-wavelet derived surrogate respiration. The average respiration accuracy which can be calculated looking at zero-crossing intervals, and the RSA, calculated by looking at the respiratory rate, both compared with respect to real respiratory parameters are used to compare results obtained using the ECG and heart sounds. From the results presented in Table 1, we can say with further assurance that heart sounds can serve as a suitable source for extracting respiratory information.

The results from different experiments are also summarized using box plots in Fig. 26-31. 'Q1' is first quartile value (0-25th percentile) data point of each sample set. 'Min' is the minimum value of the sample set. 'Median' is the median percentile value of the sample set. 'Max' is the maximum value of the sample set. 'Q3'is the third quartile value (75th – max percentile) of the sample set.

Legends: RS: Respiration derived from heart sounds (ensemble averaging) compared with respiration

EMD-HSR: Heart sound derived respiration obtained using EMD compared with real respiration

EDR: EDR derived from EMD compared with respiration

WDR: EDR derived from wavelets compared with respiration

Figures 26-31 show the box plots for the zero crossing intervals, peak to peak intervals and RSA correlation values compared with real respiration across supine and upright categories. Even though the wave to wave correlation for respiration derived from heart sounds is not as good as that obtained from wavelets (with the real respiratory signal), other pertinent factors like the frequency accuracy (zero crossing intervals) , peak to peak intervals and respiratory rate (RSA) outperform or equal both EDR techniques.

Table 1: Correlation analysis of four categories of derived respiration signals and their parameters compared with the measured respiration signal parameters

		Zero Crossing	RSA	Correlation	Peak to peak
	RS vs Respiration	0.87	0.83	0.36	0.89
Supine	EMD vs Respiration	0.83	0.79	0.26	0.83
	WDR vs Respiration	0.78	0.79	0.55	0.88
	EMD-HS vs Respiration	0.82	0.8	0.13	0.815
	RS vs Respiration	0.84	0.83	0.32	0.87
Upright	EMD vs Respiration	0.82	0.78	0.18	0.85
	WDR vs Respiration	0.83	0.74	0.55	0.8531
	EMD-HS vs Respiration	0.76	0.84	0.16	0.78

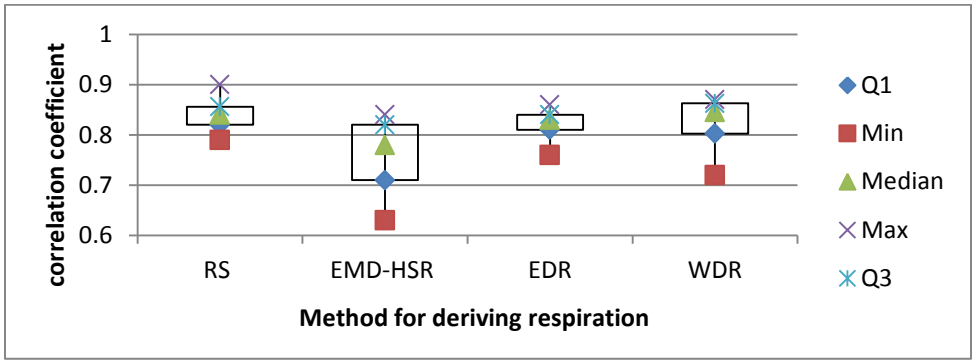

Figure 26: Comparison of box plots from various methods and measurements for zero crossing intervals in upright samples. The horizontal axis shows the various signals used in the analysis compared with respect to the real respiration. The vertical axis shows the correlation coefficients

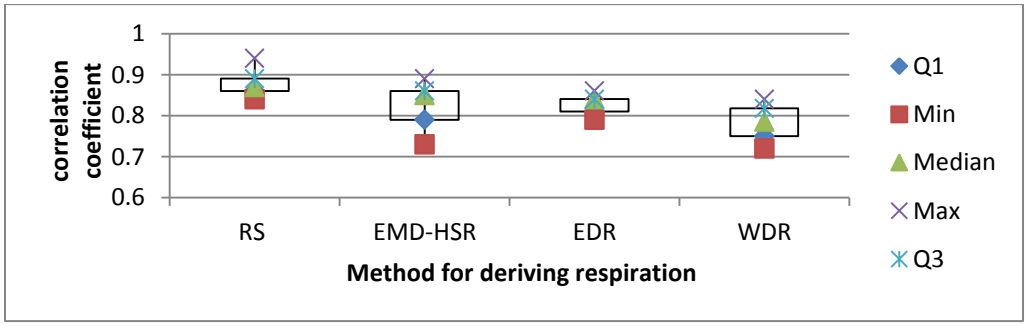

Figure 27: Comparison of box plots from various methods and measurements for zero crossing intervals in supine samples. The horizontal axis shows the various signals used in the analysis compared with respect to the real respiration. The vertical axis shows the correlation coefficients

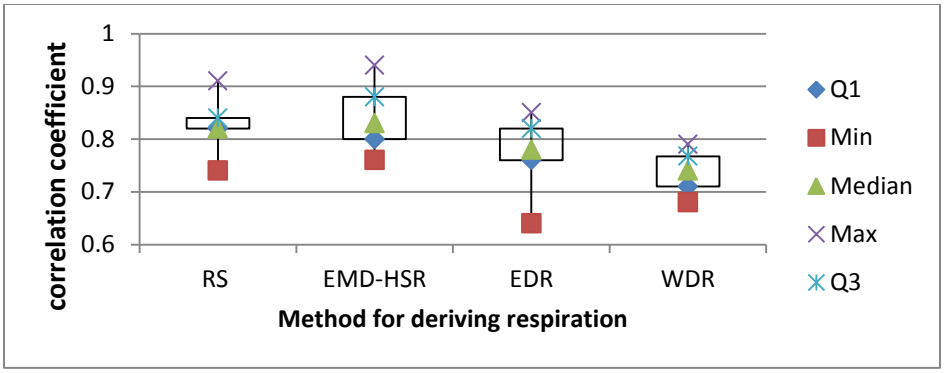

Figure 28: Comparison of box plots from various methods and measurements for RSA in Upright samples. The horizontal axis shows the various signals used in the analysis compared with respect to the real respiration. The vertical axis shows the correlation coefficients

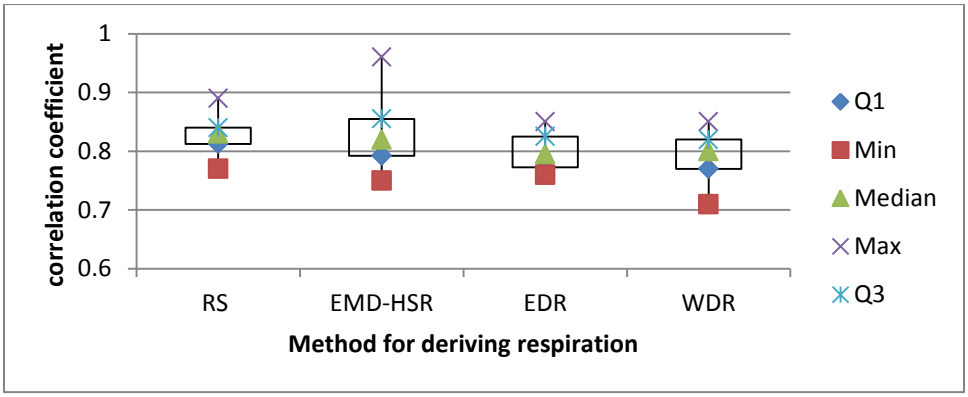

Figure 29: Comparison of box plots from various methods and measurements for RSA in Supine samples. The horizontal axis shows the various signals used in the analysis compared with respect to the real respiration. The vertical axis shows the correlation coefficients

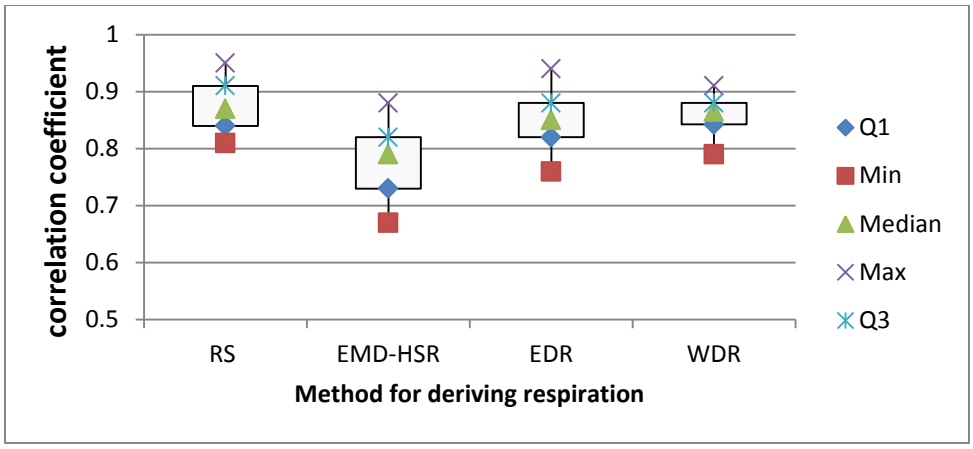

Figure 30: Comparison of box plots from various methods and measurements for peak to peak intervals for upright samples. The horizontal axis shows the various signals used in the analysis compared with respect to the real respiration. The vertical axis shows the correlation coefficients

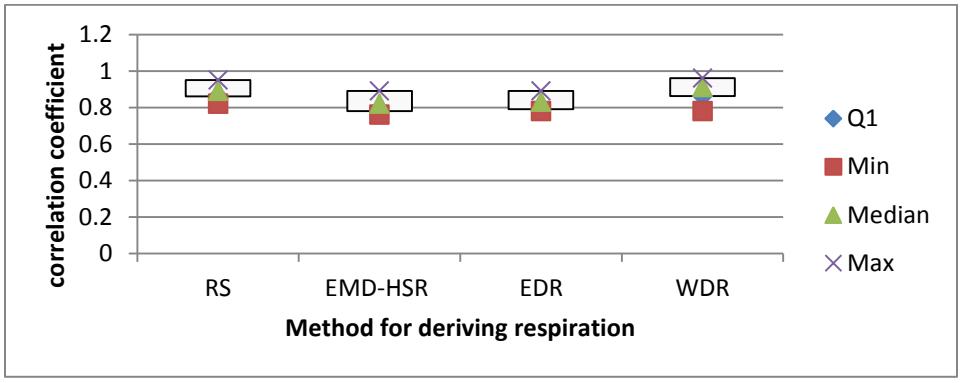

Figure 31: Comparison of box plots from various methods and measurements for peak to peak intervals for supine samples. The horizontal axis shows the various signals used in the analysis compared with respect to the real respiration. The vertical axis shows the correlation coefficients

This chapter compared the results obtained using the derived respiration signals with the measured respiration signal waveforms. The heart sound derived respiration shows promising results ($\rho > 80\%$) when compared with measured respiration parameters. Further research should be pursued, involving calculating heart sound derived respiration, which could open up newer avenues for estimating respiration derived parameters.

CHAPTER VI

PREDICTING SLEEP APNEA USING RESPIRATION INFORMATION

Sleep apnea is a common disorder in which a person has shallow breaths or one or more pauses in breathing during sleep. An apnea is defined in adults as the cessation of airflow for 10 or more seconds [56]. Breathing pauses can last from a few seconds to minutes. They often occur 30 times or more during an hour [54]. It is estimated that 12-18 million Americans are affected by sleep apnea [57]. The following table gives some statistics regarding the severity of this disorder in the United States.

Table 2: US Sleep Apnea Statistics [58]

US Sleep Apnea Statistics				
Number of Americans affected by sleep Apnea	Percentage of Americans having undiagnosed Sleep Apnea	Number of Americans having undiagnosed Sleep Apnea	% of Patients over 40 years of age having SA	% of middle-aged women having SA
18 million	6.62%	5.4 million	50% of all apnea cases are diagnosed in patients with over 40 years of age	2 to 4%

Approximately 1 in 15 or 6.62% or 18 million people in the USA believed to have sleep apnea with over 50% of all apnea cases being diagnosed in patients with more than 40

years of age. SA is found to be more prevalent in men than women. It has been observed that 4 to 9% of middle-aged men and 2 to 4% of middle-aged women suffer from sleep apnea [58].

In particular, there are two types of sleep apnea viz., obstructive sleep apnea (OSA) and central sleep apnea (CSA). OSA is characterized by periodic complete or partial upper airway obstruction during sleep, causing intermittent cessations of breathing (apneas) or reductions in airflow (hypopneas) despite ongoing respiratory effort [55]. Total costs attributed to the treatment of OSA stand at $3.4 billion [59]. When a person tries to breathe, any air that squeezes past the obstruction can cause loud snoring. Obstructive sleep apnea is more common in people who are overweight, but it can affect anyone [54]. Central sleep apnea (CSA) is a less common type of sleep apnea. This disorder happens if the area of the brain that controls breathing doesn't send the correct signals to the breathing muscles. As a result, the subject makes no effort to breathe for brief periods. Central sleep apnea often occurs with obstructive sleep apnea, but it can occur alone. Snoring doesn't typically happen with central sleep apnea [54]. Polysomnography is increasingly being used to investigate patients with possible sleep apnoea/ hypopnoea syndrome (SAHS). Apnea-Hypopnea Index (AHI) results are used to diagnose sleep apnea. AHI levels between 5-15 are termed mild sleep apnea; people with levels between 15 and 30 are classified as having moderate sleep apnea, while those having levels more than 30 are classified as having severe sleep apnea [60].

As the respiration pattern is affected during apnea, understanding respiration rate becomes vital in order to predict the occurrence of sleep apnea. This chapter attempts to address this problem using advanced predictive modeling tools like neural networks,

regression, and decision trees. The Physionet's Apnea-ECG database consists of a collection of samples containing ECG, SpO2 content and three variants of respiration information viz., chest respiration, abdomen respiration and nasal respiration [61]. Annotations specifying apneic/non-apneic periods are also included. Fig. 32 is a ten second representation of Physionet's Apnea ECG database signal (a01er). This signal was recorded for more than eight hours at a sampling rate of 100 Hz.

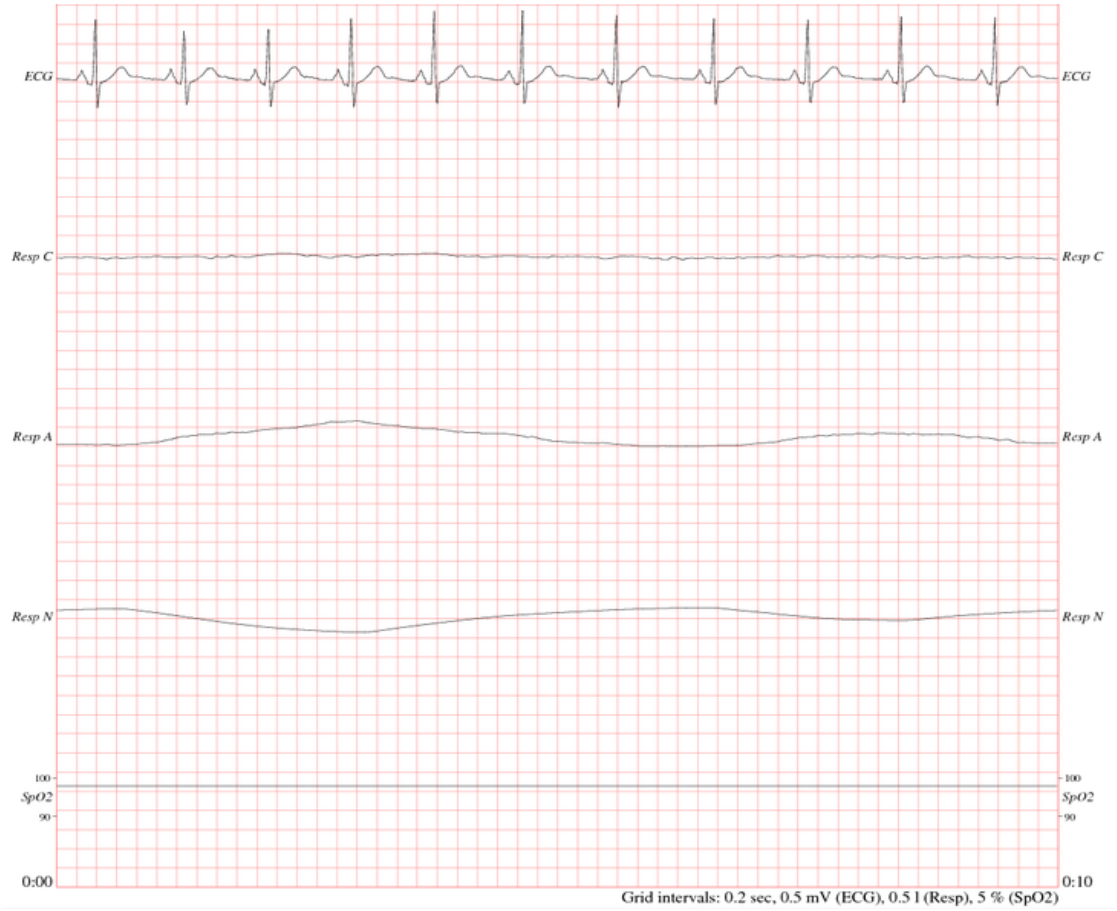

Fig 32: A representative collection of signals consisting of ECG, Chest respiration, Abdomen respiration, Nasal respiration and SpO2 content is presented [61]. The recorded signal is 10 seconds in length.

The signal records ECG, Chest respiration, Abdomen Respiration, Nasal Respiration along with SpO2 content. The data sample also consists of apnea annotations at 1 minute intervals. These annotations were considered a target variable for further analysis. The Predictive Modeling toolbox in SAS Enterprise Miner was used for analyzing signals in order to predict sleep apnea onset. Apart from respiration signals, heart rate represented in beats per minute (BPM) was also estimated by calculating the RR intervals in the ECG signal. The target variable (apnea annotations) was recoded into a binary representation with apneic episodes represented by a string of 1's and non-apneic periods represented as a string of 0's. As the respiration signals have a time series component, the nasal respiration signal along with its ten time lagged versions ranging from a lag of ten samples to 100 samples respectively, were included as input variables in the analysis. ECG and SpO2 variables were rejected.

6.1 Data Modeling

The dataset was combined with these input variables as well as target variables included in the final dataset used for modeling. Fig. 33 depicts the steps involved in classifying sleep apnea. The procedure involves a total of five steps comprising preparing a dataset suitable for use, oversampling of target variable, data partitioning for validation, application of predictive models like decision trees, neural networks, and regression and finally comparison within these models.

As the target variable consists of an unequal proportion of 0's and 1's, there is a possibility that it might bias the results of the model. In order to remove this uncertainty,

we employ an oversampling method in order to obtain a sample consisting of equal numbers of 0's and 1's.

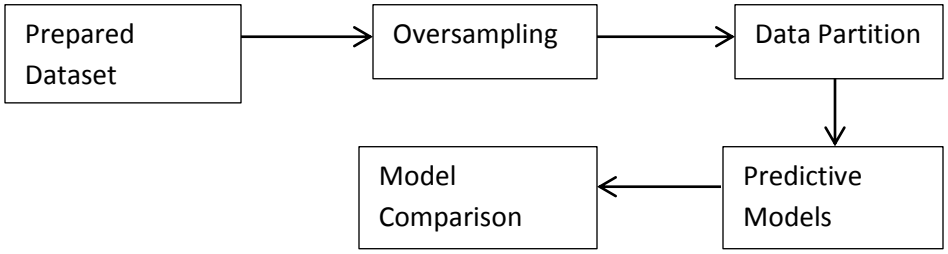

Fig. 33: A block diagram explaining steps involved in classifying onset of sleep apnea.

Further, 50 % of the sample data is partitioned for calibration or training, while the remaining 50 % is used for validating the trained model. Different predictive modeling tools, such as decision trees, neural networks and regression analysis were used to predict the onset of apnea (Target=1). Appendix 1 shows the modeling procedure used in SAS Enterprise Miner. Apart from these modeling tools, an ensemble node was also used for comparison. This node generates results which are an average of all the results calculated by other predictive modeling tools. The results obtained after running these models are compared to select the best model. The best model is selected based on lowest misclassification rate.

6.2 Results of preliminary analysis

The results obtained using the preliminary model and the recurrence models that follow this model are based on four metrics: Validation Misclassification Rate, Lift, Sensitivity and Specificity. The definitions of the following variables are as follows:

1. **Misclassification Rate**: Rate at which misclassification occurs in the validation data (Misclassification occurs when the predicted target value is not equal to the actual target value).
2. **Lift:** Lift indicates the improvement provided by the model with respect to the baseline (random guess probability).

3. **Sensitivity**: Sensitivity is defined as a ratio of true positives (TP) to the sum of true positives and false negatives (FN)

$$\text{Sensitivity} = \frac{TP}{(TP+FN)} \tag{13}$$

   Where, TP is the number of true values correctly predicted (Predicted True as True), FN is the number of true values predicted as false.

4. **Specificity**: Specificity is defined as a ratio of true negatives (TN) to the sum of true negatives and false positives (FP)

$$\text{Sensitivity} = \frac{TN}{(TN+FP)} \tag{14}$$

   Where, TP is the number of true values correctly predicted (Predicted False as False), FN is the number of false values predicted as true.

Results generated by the models are listed in Table 3.

The best model was the model which used the AutoNeural node settings in SAS Enterprise Miner (see Appendix 2). The AutoNeural node is an automated tool which

finds the optimal configurations of a neural network model based on various feed forward network configurations [62]. The AutoNeural node provides a lift of 1.97 over the baseline, which indicates that we can classify the apneic episode 1.97 times better than the base probability. Fig. 34 gives a graphical representation of sensitivity vs. the false positive ratio for all the models used in the analysis. The baseline is represented by the 45 degree line. All models are compared with respect to the baseline model.

Table 3: Results generated by different models used in SAS Enterprise Miner for preliminary analysis

Selected Model	Model Description	Validation Misclassification Rate	Lift
Y	Auto Neural	0.1091	1.97764
	Ensemble	0.115858	1.9248
	Neural Network	0.14077	1.8312
	Decision Tree	0.145737	1.8656
	Regression	0.285674	1.7784

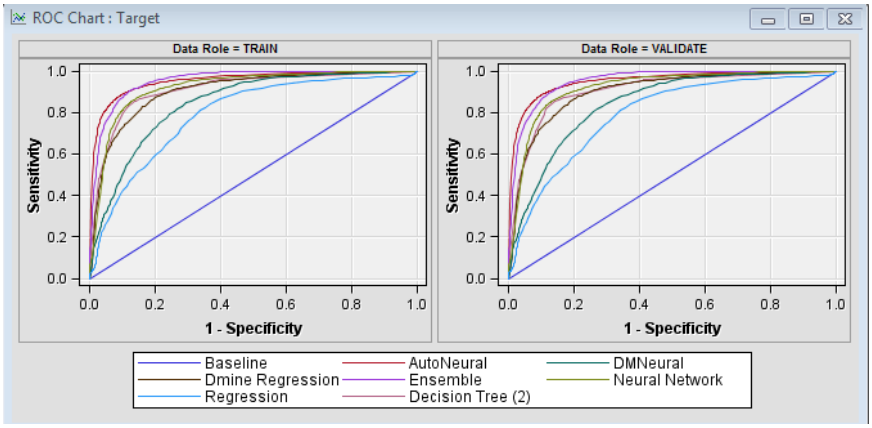

Fig 34: ROC index chart showing the sensitivity vs. 1-specificity ratio for preliminary analysis

The sensitivity and (1-specificity) values are plotted against each other across every percentile. The plot obtained by joining these points is represented in the ROC chart. An ROC index greater than 0.7 is considered to be a strong model. The validation ROC index for this model= 0.95, which indicates that the model is robust. Table 4 shows the sensitivity and specificity ratios for the different models used in the analysis.

Table 4: Table of sensitivity and specificity ratios for preliminary analysis

Model	Sensitivity	Specificity
Neural network	84.84%	87%
Regression	70.25%	72.60%
AutoNeural	88.11%	90.04%
Decision Tree	85.16%	85.68%
Ensemble`	89.32%	87.5%

The AutoNeural model which came out to be the best model in terms of misclassification rate shows a sensitivity of 88.11% and a sensitivity of 90.04% .

6.3 Recurrence Analysis

The study of dynamic systems is the study of the long-term behavior of evolving systems [64]. Dynamic systems are characterized by mathematical models where a fixed rule underlies the time dependence of a point in a geometric space. For example, the swinging of a pendulum is quantified by an underlying pattern that can be characterized as a dynamic system. Recurrence is a fundamental property of dynamical systems, a property which can be exploited to characterize the system's behavior in the phase space [63]. A recurrence plot (RP) is a powerful tool for visualization and analysis of recurrence patterns [63]. RP's were originally posited as qualitative tools to detect hidden rhythms graphically [66]. Webber et.al [65] explain recurrence by considering a system of literal waves on the seas as measured from buoy instrumentation, as plotted in Fig. 35. The figure indicates that each of the waves (of the same height) in (A) are recurrent with one another at time instances which are non- periodic. In order to go beyond the visual impression yielded by RP's, recurrence quantification analysis (RQA) uses several measures of complexity for quantifying small scale structures in RP's [63]. These measures are based on the recurrence point density and the diagonal and vertical line structures of the RP [63]. In this study, the respiration rate derived by applying EMD on ECG signals and heart rate variability derived as a measure of RR intervals were processed using RQA. Besides RR intervals, we also input the RQA model with the following parameters:

1. Dimension M=7
2. Delay T=5

3. Size of neighborhood $E = 0.1 * [\max(Amplitude) - \min(Amplitude)]$
4. Window size $W = 60 * 10$
5. Shifting Window Size: $60 * 1$
6. Minimal Length of diagonal line structure: $L_{min} = 3$
7. Minimal Length of vertical line structure: $V_{min} = 3$
8. Theiler Window : $TW = 1(default)$

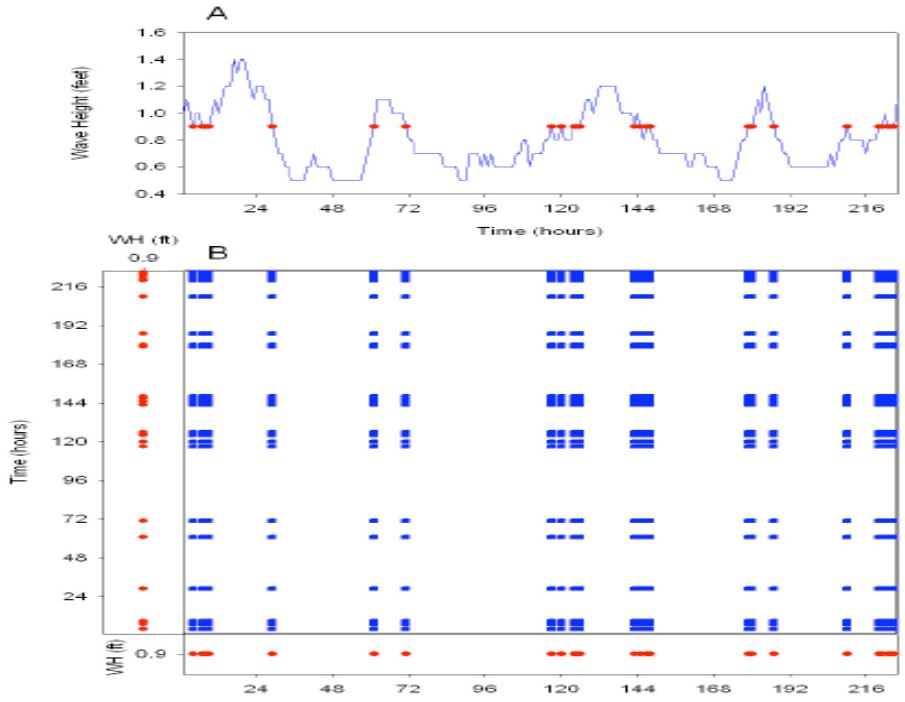

Fig. 35: A typical recurrence plot [65] is shown in (B) above which captures points at wave height of 0.9 ft identically represented along vertical and horizontal axes. The horizontal and vertical axes represent time in hours. Only the intersecting pixels mapping our matches at 0.9ft are represented while all other pixels are ignored.

The results yielded 13 features (see Appendix 4) which are fed as an input to the predictive analysis model in SAS Enterprise Miner to predict sleep apnea. Some of the important outputs measured are described below:

1. **Recurrence Rate**: It is a measure of density of recurrence points in the RP

It is the probability that a state occurs in a Ɛ- neighborhood in phase space.

$$RR(\epsilon) = \frac{1}{N^2} * \sum_{i,j=1}^{N} R_{i,j}(\epsilon) \quad (15)$$

2. **Determinism**: Determinism(DET) is defined as the ratio of recurrence points that form the diagonal structures (of at least length (l_{min})to all recurrence points

$$\text{DET} = \frac{\sum_{l=l_{min}}^{N} l\, P(l)}{\sum_{l=1}^{N} l\, P(l)} \quad (16)$$

3. **Mean diagonal line length** : The mean diagonal line length (L) is defined as the average time that two segments of a trajectory are close to each other, and can be predicted as the mean prediction time.

$$L = \frac{\sum_{l=l_{min}}^{N} l\, P(l)}{\sum_{l=lmin}^{N} P(l)} \quad (17)$$

4. **Longest diagonal length**: It is the longest diagonal length found in the RP.

$$L_{max} = \max(\{l_i\}_{i=1}^{N_l}) \quad (18)$$

5. **Entropy**: Entropy (ENTR) reflects the complexity of the RP with respect to the diagonal lines. For example, the entropy of uncorrelated white noise is small, indicating low complexity.

$$ENTR = -\sum_{l=l_{min}}^{N} p(l)\, ln\, P(l) \quad (19)$$

6. **Laminarity**: Laminarity (LAM) is defined as a ratio between the recurrence points forming the vertical structures and the entire set of recurrence points that can be computed.

$$LAM = \frac{\sum_{v=v_{min}}^{N} v\, P(v)}{\sum_{v=1}^{N} v\, P(v)} \quad (20)$$

7. **Trapping time**: It is defined as the average length of the vertical structures. It indicates the mean time a system will abide in a particular state.

$$TT = \frac{\sum_{v=v_{min}}^{N} v\, P(v)}{\sum_{v=v_{min}}^{N} P(v)} \quad (21)$$

8. **Maximal length of vertical lines**: It can be regarded analogously to the standard measure L_{max}. N_v is the absolute number of vertical lines.

$$V_{max} = \max(\{v_l\}_{l=1}^{N_v}) \quad (22)$$

Following there models were run in total, two of which consisted of respiration rate and heart rate variability as separate models, while the third model included both respiration rate and HRV as inputs in order to predict the onset of sleep apnea characterized by apnea annotations used in Chapter 6.2. The models have been summarized in Table 5

Table 5: Summary of models:

Model	Input
Model 1	RQA features of respiratory rate
Model 2	RQA features of HRV
Model 3	RQA features of both HRV and respiratory rate

6.4 Results obtained using RQA for Model 1(Respiration features)

Table 6 and 7 show the results obtained by using five predictive models on the target (sleep apnea annotations). The Respiration rate features obtained using RQA were processed using Principal Component Analysis (PCA). Principal component analysis was used to reduce the multi-collinearity among the input variables. Fig. 36 shows a representative figure showing variables transformed into its principal components.

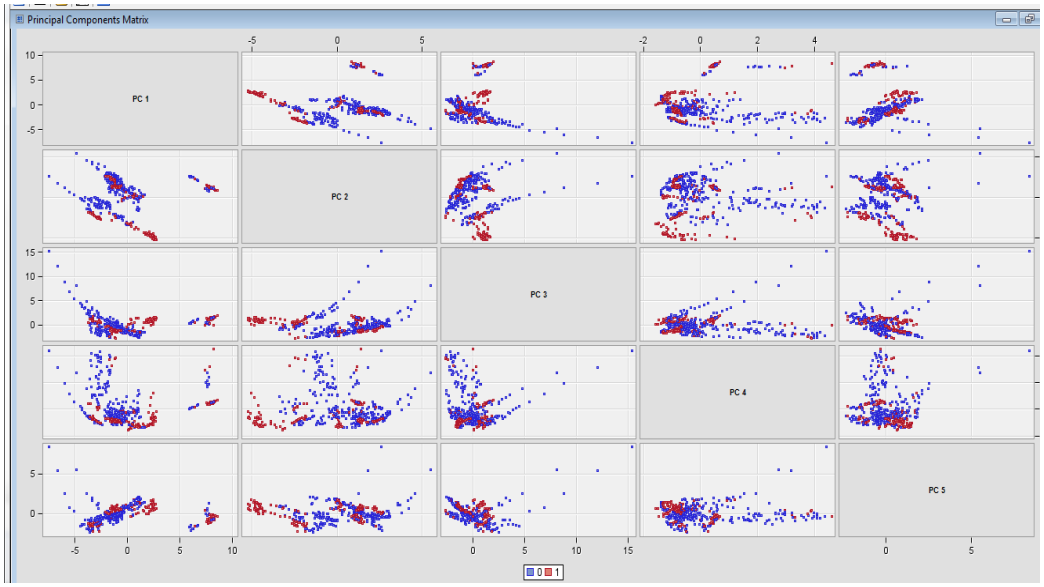

Fig 36: Principal components matrix showing representation of all variables with respect to target

Seven PC's out of 12 were selected which accounted for 99% of the total cumulative variance. The sensitivity and (1-specificity) values are plotted against each other across every percentile. The plot obtained by joining these points is represented in the ROC chart in Fig. 37

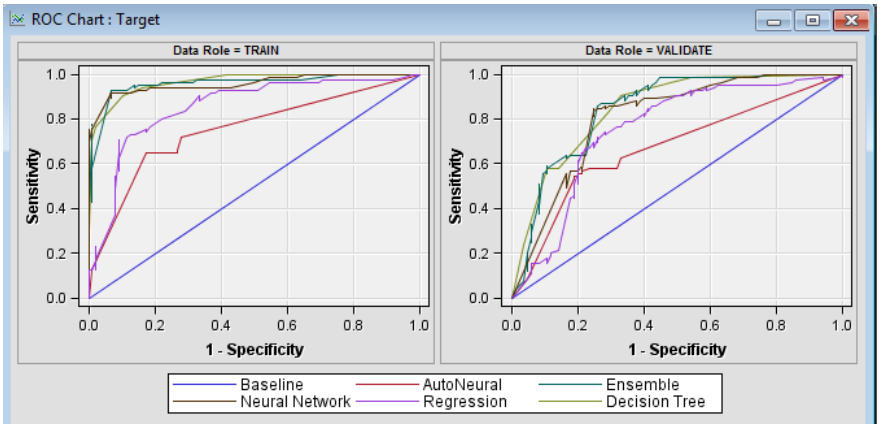

Fig 37: ROC index chart showing the sensitivity vs. 1-specificity ratio for model 1

An ROC index of greater than 0.7 is considered to indicate strong models. The validation ROC index for this model is 84.7%, which indicates that the model is robust.

Table 6: Table of sensitivity and specificity ratios

Model	Sensitivity	Specificity
Neural network	84.7%	75.29%
Regression	70.58%	74.11%
AutoNeural	57.64%	76.47%
Decision Tree	83.52%	70.58%
Ensemble`	87.05%	75.29%

Based on the model comparison results, the Ensemble model has the lowest misclassification rate and therefore is the best model. Figure 38 shows the representation of the target variable for both the model prediction and in the original dataset. The horizontal axis represents time in minutes while the vertical axis represents the state of the binary variable.

A

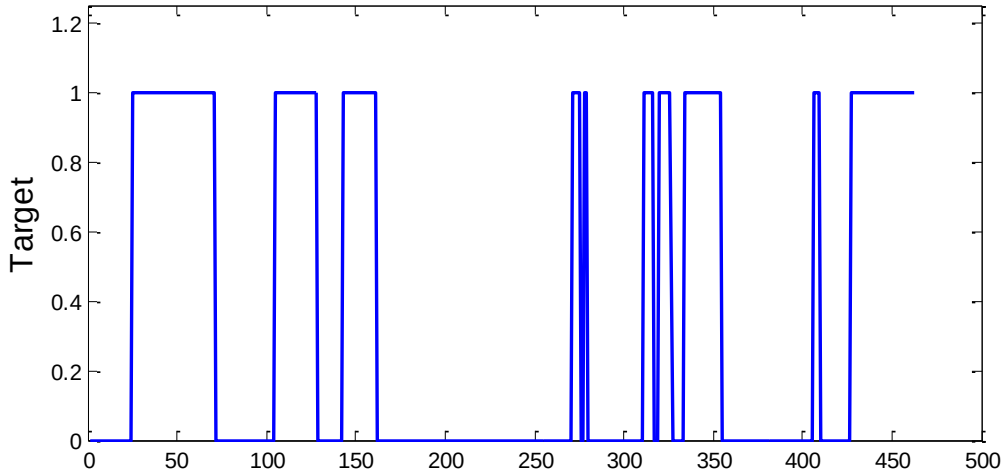

B

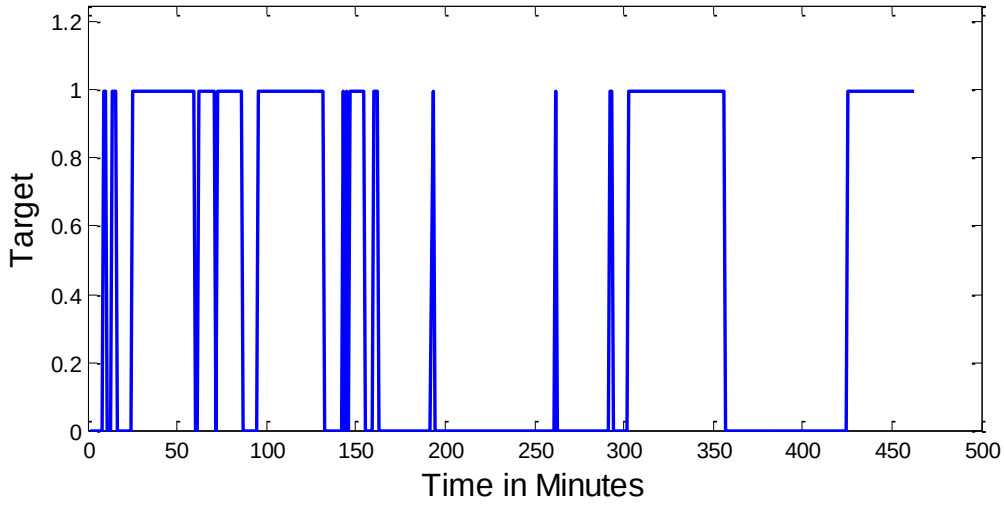

Fig 38: Target distribution in (a) original dataset for respiration rate (b) predicted dataset

Table 7: Results generated by different models used in SAS Enterprise Miner

Selected Model	Model Description	Validation Misclassification Rate	Lift
Y	Ensemble	0.2	1.75
	Neural Network	0.2	1.5
	Tree	0.2294	1.73
	Regression	0.2401	1.25
	AutoNeural	0.3294	1.56

6.5 Results obtained using RQA for Model 2 (HRV features)

Tables 8 and 9 show the results obtained by using five predictive models on the target (sleep apnea annotations). The respiration rate features obtained using RQA were processed using Principal Component Analysis (PCA). Principal component analysis was used to reduce the multi-collinearity among the input variables. Seven PC's out of 12 were selected which accounted for 99% of the total cumulative variance.

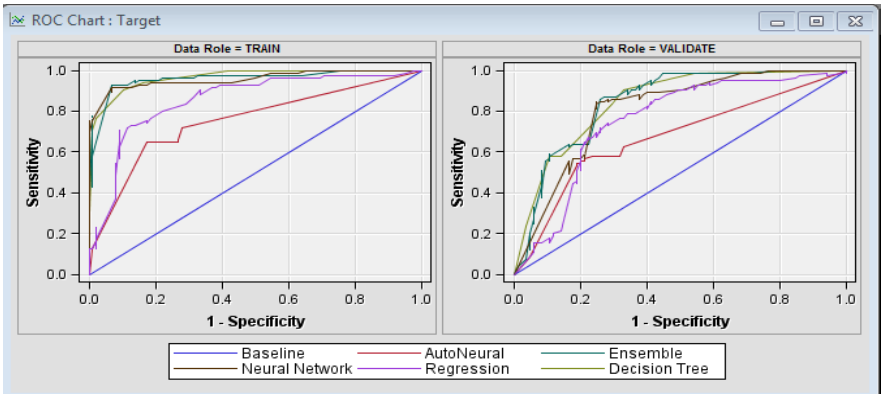

Fig 39: ROC index chart showing the sensitivity vs. 1-specificity ratio for model 2

The sensitivity and (1-specificity) values are plotted against each other across every percentile. The plot obtained by joining these points is represented in the ROC chart. An ROC index of greater than 0.7 is considered to indicate strong model. The validation

ROC index for this model is 89.9%, which indicates that the model is robust. Based on the model comparison results, the Auto Neural model has the lowest misclassification rate and therefore is the best model.

Table 8: Table of sensitivity and specificity ratios

Model	Sensitivity	Specificity
Neural network	80%	80%
Regression	70.58%	82.35%
AutoNeural	96.47%	84.7%
Decision Tree	75.29%	81.1%
Ensemble`	81.1%	82.35%

Table 9: Results generated by different models used in SAS Enterprise Miner

Selected Model	Model Description	Validation Misclassification Rate	Lift
Y	AutoNeural	0.14	1.25
	Ensemble	0.18	1.5
	Neural Network	0.2	2
	Decision Tree	0.21	1.71
	Regression	0.23	2

Figures 40 show the representation of the target variable for both the model prediction and as seen in the original dataset. The horizontal axis represents time in minutes while the vertical axis represents the state of the binary variable.

A

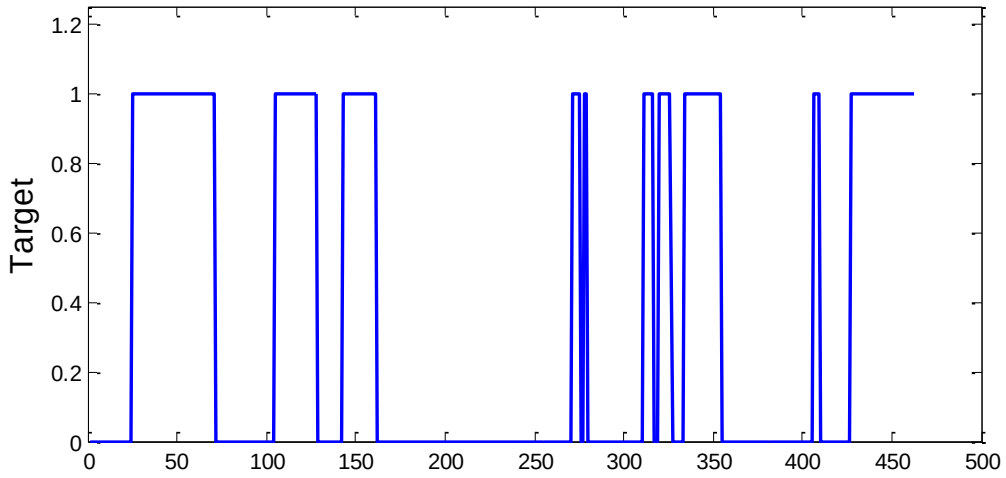

B

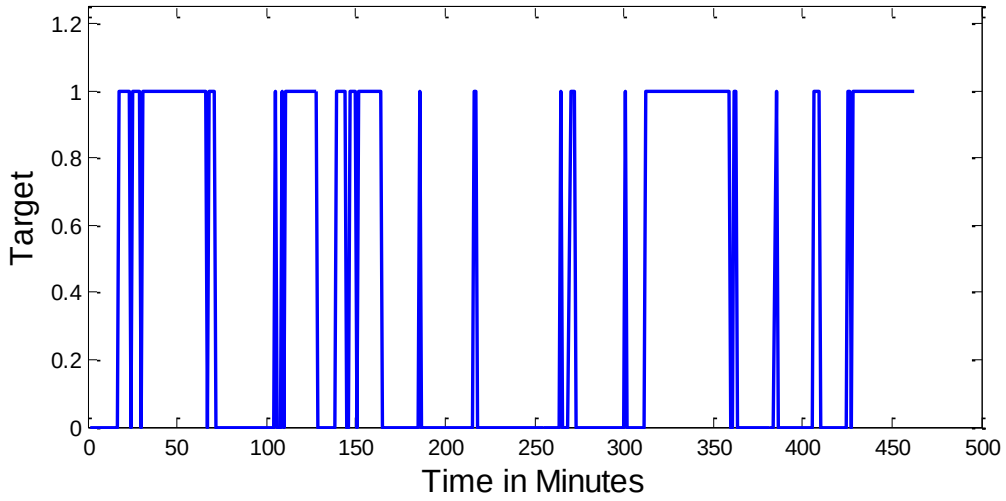

Fig 40: HRV target distribution in (a) Original dataset and (b) Predicted dataset

6.6 Results obtained using RQA for Model 3(Respiration rate and heart rate features)

Two types of tests were conducted to develop and validate model 3. In the first case, respiration and heart rate features were directly used as inputs to the classification model

and in the second case, ten permutations of respiration and heart rate features were used as inputs to the classification model. The sleep apnea annotations were used as a target which is binary in nature. Auto Neural node, decision trees, neural network and regression apart from ensemble averaging node were used to classify sleep apnea. The settings have been listed in the appendix.

Case 1 results:

The sensitivity and (1-specificity) values are plotted against each other across every percentile in Fig. 43. The plot obtained by joining these points is represented in the ROC chart. An ROC index greater than 0.7 is considered to be a strong model. The validation ROC index for this model is 94.9%, which indicates that the model is robust.

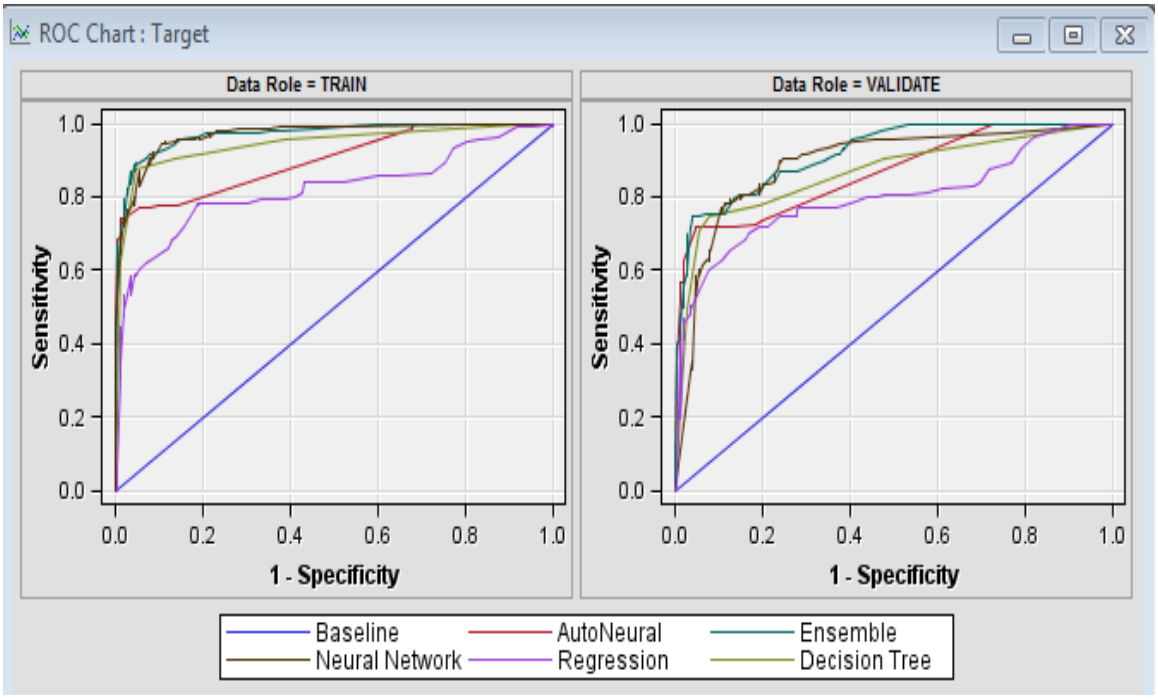

Fig 41: ROC index chart showing the sensitivity vs. 1-specificity ratio for model 1

Tables 10 and 11 show the results obtained using five predictive models on the target (sleep apnea annotations)

Table 10: Table of sensitivity and specificity ratios for model 3

Model	Sensitivity	Specificity
Neural network	87.09%	81.13%
Regression	75.8%	87.73%
AutoNeural	91.93%	85.84%
Decision Tree	72.58%	92.45%
Ensemble`	83.87%	71.7%

Based on the model comparison results, a decision tree was found to be the best model considering it had the lowest misclassification rate.

Table 11: Results generated by different models used in SAS Enterprise Miner for model 3

Selected Model	Model Description	Validation Misclassification Rate	Lift
Y	AutoNeural	0.1194	2.7
	Decision Tree	0.1563	2.7
	Ensemble	0.1577	2.6
	Neural Network	0.1664	2.3
	Regression	0.1729	1.89

The HRV and respiration rate features obtained using RQA were processed using principal component analysis (PCA). Principal component analysis was used to reduce the multi-collinearity among the input variables.

Thirteen PC's out of 24 were selected and accounted for 99% of the total cumulative variance (Refer to Appendix 3). Figures 42 show the representation of the target variable for both the model prediction and as seen in the original dataset. The horizontal axis represents time in minutes while the vertical axis represents the state of the binary variable. To further test the validity of the model, we divided the dataset into two datasets: one having data from 12 samples out of 15, while the other having data from the remaining three samples. The dataset containing remaining three samples are used to score the model built using the dataset containing 12 samples.

A

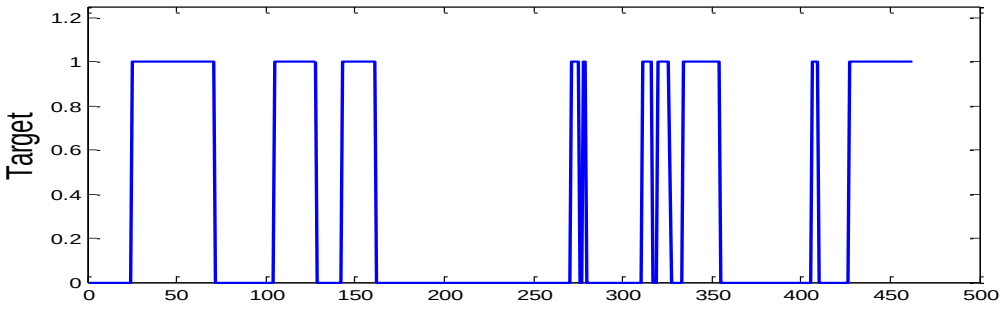

B

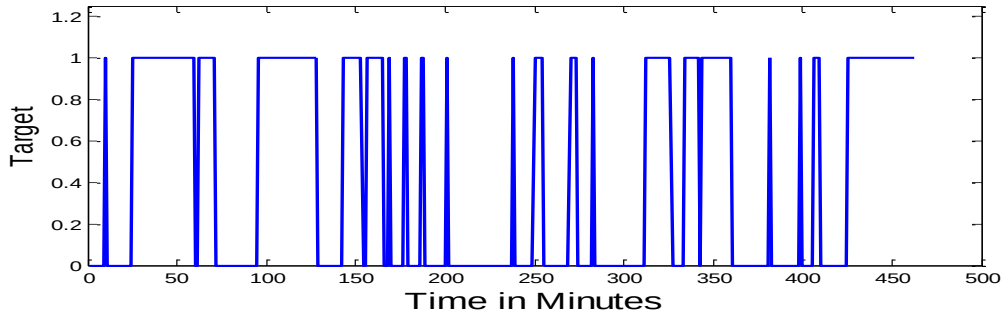

Figure 42: (a) Target distribution for both respiration rate and heart rate features in model three and (b) Predicted distribution for both respiration rate and heart rate features in model 3

Case 3 results:

This procedure is repeated for ten independent data permutations of the 12 sample dataset. The results obtained for the best classification model (AutoNeural) suggested that the validation misclassification rate was 8.9%. Based on these results, we can state with improved confidence, that the model built earlier was robust.

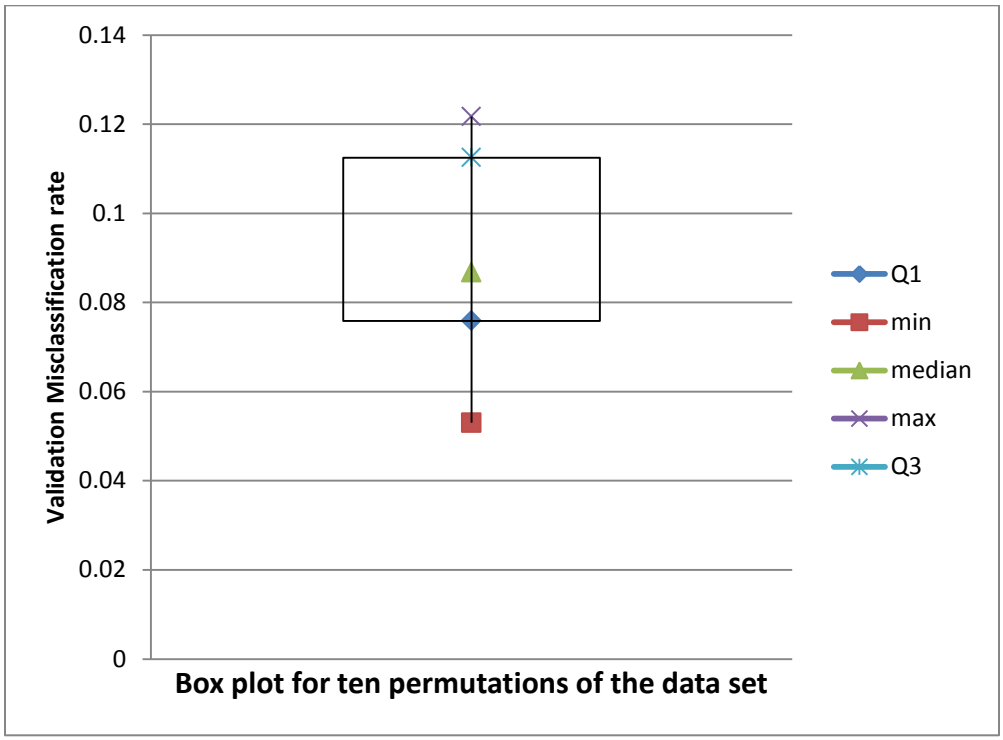

Figure 43. Box plots for the ten permutations

Decision analysis based filtering:

The transitions that last for less than 60 sec are likely to be artifacts. Therefore, we developed a rule to disregard these double transitions. The results from such a filtering are summarized in Fig. 47.

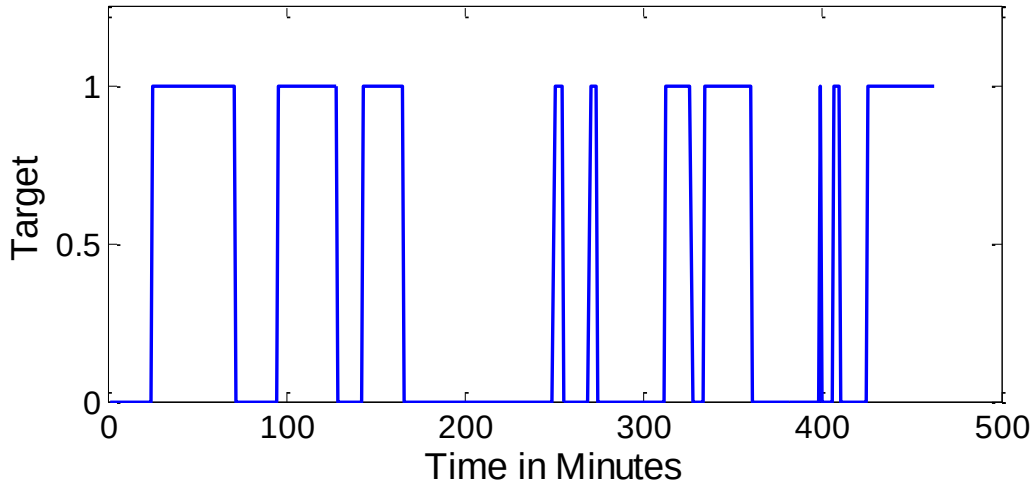

Figure 44: Decision based filtering procedure on predicted dataset

6.7 Model Comparison of all four models

The Table 12 below and Figs. 45-48 describe all four models (Best model in each category) with respect to the sensitivity, specificity, lift and misclassification rate parameters. Preliminary Analysis Model stands out in two out of four categories. Also, the sensitivity and specificity values are stable in preliminary analysis model.

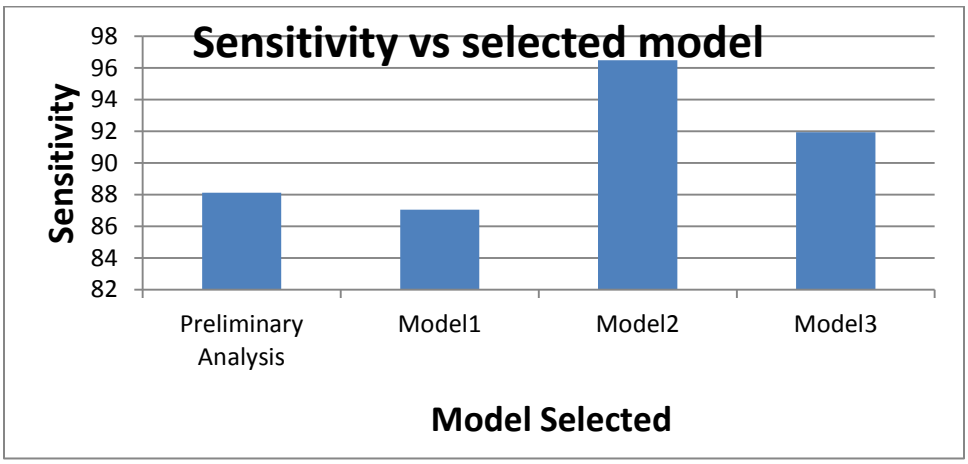

Fig 45: Sensitivity vs Selected Model. Best model based on sensitivity is model 2

Table 12: Model comparison

	Sensitivity	Specificity	Lift	Misclassification Rate
Preliminary Analysis	88.11	90.04	1.97	0.1091
Model 1 (Respiration rate)	87.05	75.29	1.75	0.2
Model 2 (HRV)	96.47	84.7	1.25	0.14
Model 3 (HRV and Respiration Rate)	91.93	85.84	2.7	0.1194

Fig. 45 shows a plot of Sensitivity against Selected Model for all four models used. Based on these results, the model that would be selected based on the sensitivity criterion only, is Model 2 which is a recurrence analysis of heart rate variability.

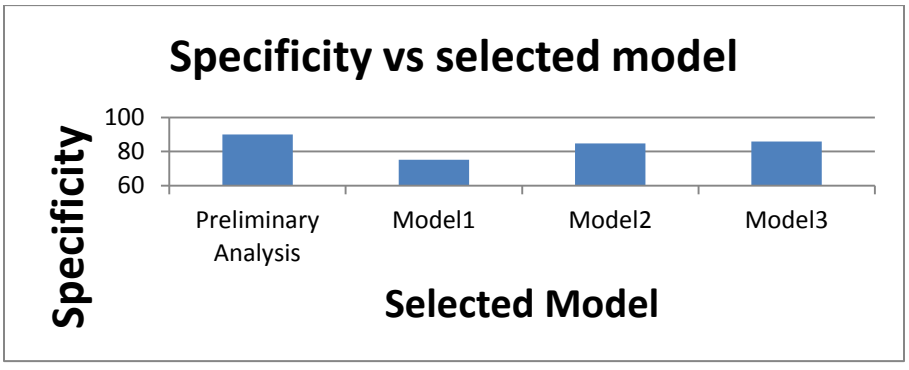

Fig 46: Specificity vs Selected model. Best model selected is Preliminary Analysis.

Fig. 46 shows a plot of Specificity against Selected Model for all four models used. Based on these results, the model that would be selected based on the specificity criterion only, is Preliminary analysis which is a recurrence analysis of both the respiration and heart rate variability.

Fig. 47 shows a plot of Lift against Selected Model for all four models used. Based on these results, the model that would be selected based on the lift criterion only, is the Model 3.

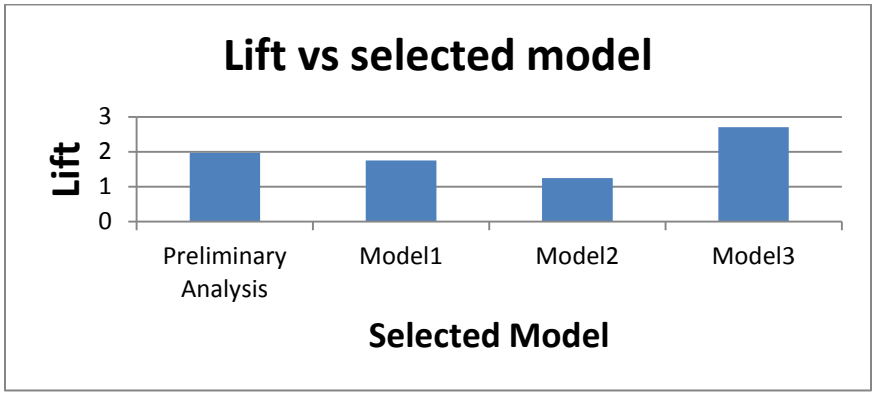

Fig 47: Lift vs Selected Model. Best model selected is Model 3

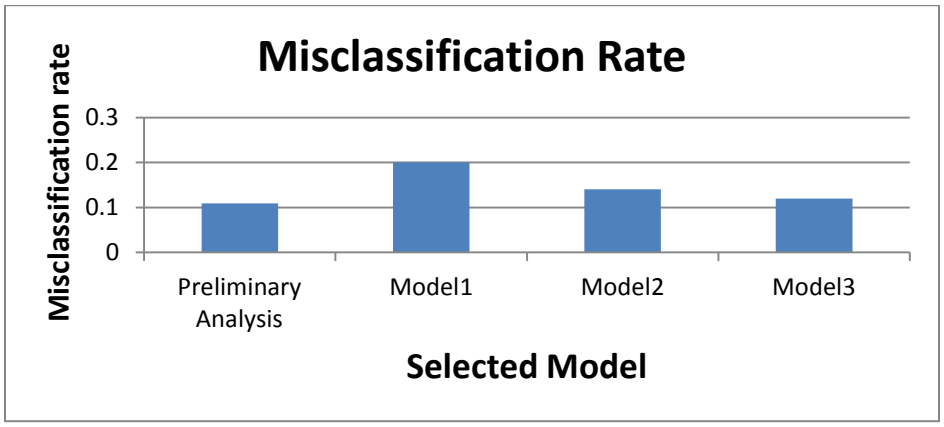

Fig 48: Misclassification Rate vs Selected Model. Best Model selected is Preliminary Analysis

Fig. 48 shows a plot of misclassification rate against Selected Model for all four models used. Based on these results, the model that would be selected based on the misclassification criterion only, is the Preliminary analysis model.

Chapter 6 touched upon an important application of estimating respiratory rate to classify sleep apnea. Similarly, respiration information could also be used to understand cardiovascular dynamics better, as many heart diseases have been linked with respiration as talked about before.

CHAPTER VII

SUMMARY

This thesis proposes, a respiration extraction algorithm using phonocardiogram signals that employs the technique of ensemble averaging to derive respiration. The respiration waveform obtained by applying this algorithm to the phonocardiogram signals was found to contain a higher correlation with the real respiration than the respiration waveform extracted using ECG methods. The method is simple to use and could provide a low cost alternative to the popular ECG diagnosis.

The important findings from this study are as follows:

1. A method to derive respiration from heart sounds is presented, and the new method was found to match the real respiration signal better than the traditional ECG methods in terms of respiratory frequency accuracy and respiratory rate.

2. On average, the correlation between respiration waveforms derived from heart sounds with respect to the measured respiration is 36% and 32% for supine and upright samples respectively, compared to 26% and 18 % for EMD derived EDR and 55% each for wavelet derived EDR.

3. On average, the correlation between frequency accuracy for respiration derived from heart sounds with respect to the real respiration is 87% and 84% for supine and upright samples respectively, compared to 83% and 82 % for EMD derived EDR and 78% and 83% for wavelet derived EDR.

4. On average, the correlation between respiration rate derived from heart sounds with respect to the real respiration is 89% and 87% for supine and upright samples respectively, compared to 83% and 85 % for EMD derived EDR and 88% and 85% for wavelet derived EDR.

5. On average, the correlation between RSA values derived from heart sounds with respect to the real respiration is 83% and 83% for supine and upright samples respectively, compared to 79% and 78 % for EMD derived EDR and 79% and 74% for wavelet derived EDR.

6. The ensemble averaging method gives better results than the EMD method on heart sounds in all categories except the RSA for upright subjects.

7. Model comparisons within the preliminary analysis model consisting of nasal respiration as well as its time lagged components and heart rate, when compared with recurrence models, shows that the model3 has a higher lift (2.7) than the recurrence models(Preliminary Analysis: 1.97, Model 1: 1.75, Model 2: 1.25)Model comparison within preliminary analysis model consisting of nasal respiration as well as its time lagged components and heart rate when compared with recurrence models shows that the preliminary analysis model has a lower misclassification rate (10%) than the recurrence models(Model 1: 20% Model 2: 14%, Model 3: 11.94%)

CHAPTER VIII

FUTURE WORK

This thesis presented an approach to predict sleep apnea using recurrence analysis. In model 1, the recurrence analysis technique was implemented on heart rate and respiration rate, derived from ECG, to extract 13 features for each signal respectively. Here, features were extracted in a separate state space independent of each other. Cross-recurrence analysis is a bivariate extension of the recurrence analysis technique, and can be used to analyze the dependencies between two different systems by comparing their states [63]. Cross-recurrence analysis could possibly be used, to understand interdependencies in the cardiorespiratory dynamics of the body, by treating the respiratory rate and heart rate in a same state space.

Sleep apnea has been linked to a variety of cardiorespiratory disorders like hypertension, sudden infant death syndrome, high blood pressure and a risk of heart attack. Detection of patterns causing sleep apnea based on the classification methods explored in this work, could possibly open opportunities for researchers to better understand and predict symptoms leading to these other disorders.

REFERENCES

1. Pincorili, F., Rossi, R., & L.Vergani. (1985). Detection of electrical axis variation for the extraction of respiratory information. *Computers in Cardiology, 12*, 499-502.

2. Madhav, K. V., Ram, M. R., Krishna, E. H., Komalla, N. R., & Reddy, K. A. (2011). Estimation of Respiration Rate from ECG, BP and PPG signals using Empirical Mode Decomposition. *IEEE*.

3. Bowers, E., Murray, A., & Langley, P. (2008). Respiratory Rate Derived from Principal Component Analysis of Single Lead Electrocardiogram. *Computers in Cardiology, 35*, 437-440.

4. Reed, T., Nancy, E., Reed, A., & Fritzson, P. (2004). Heart sound analysis for symptom detection and computer-aided diagnosis. *Simulation Modelling Practice and Theory, 12*(2), 129-146.

5. Kumar, D., Carvalho, P., Antunes, M., Paiva, R. P., & Henriques, J. (2011). Noise detection during heart sound recording using periodicity signatures. [Research Support, Non-U.S. Gov't]. *Physiol Meas, 32*(5), 599-618

6. Debbal, S. M., & Bereksi-Reguig, F. (2008). Computerized heart sounds analysis. *Comput Biol Med, 38*(2), 263-280.

7. Huang, N.E. (1998). The empirical mode decomposition and the Hilbert spectrum for non-linear and non-stationary time series analysis, Proc Royal Soc. London A, vol. 454, pp. 903-995.

8. Campolo, M., Labate, D., Foresta, F. L., Morabito, F. C., Lay-Ekuakille, A., &

Vergallo, P. (2011). ECG-derived respiratory signal using Empirical Mode Decomposition. *IEEE*.

9. Karagiannis, A., & Constantinou, P. (2009). Noise components identification in biomedical signals based on Empirical Mode Decomposition, in Proc. 9th International Conference Information Technology and Applications in Biomedicine, (ITAB 2009), pp. 1-4.

10. Yan,L., Jingyu, Y., & Yam Yeung (2009). Model-Based ECG Denoising Using Empirical Mode Decomposition, in Proc. 2009 IEEE International Conference on Bioinformatics and Biomedicine (BIBM 2009), pp. 191-196.

11. Nimunkar, A.J. & Tompkins, W.J. (2007). Averaging for Simulated Stress ECG using EMD, in Proc. 29th IEEE Annual International Conference on Engineering Biology Society (EMBS 2007), pp. 1261-1264.

12. Hong Tang, Ting Li, & Tianshuang Qiu (2010). Noise and Disturbance Reduction for Heart Sounds in Cycle-Frequency Domain Based on Nonlinear Time Scaling, IEEE transactions on biomedical engineering ,57,325-333

13. Bai.Y, & Lu,Y. (2005). The embedded digital stethoscope uses the adaptive noise cancellation filter and the type I Chebyshev IIR bandpass filter to reduce the noise of the heart sound, in Proc. 7th Int.Workshop Enterprise Networking Computers in Healthcare Industry, Busan, Korea, Jun. 23-25, 2005, pp. 278–281.

14. Gnitecki,J., Moussavi,Z., & Pasterkamp,H. (2010). Recursive least squares adaptive noise cancellation filtering for heart sound reduction in lung sounds recordings, in Proc. 25th Annu. Int. Conf. IEEE EMBS, Cancun, Mexico, Sep. 17–21, 2003, 2010, pp. 2416–2419.

15. Charlestion, S. & Azimi-Sadjadi, M. R. (1996). Reduced order Kalman Filtering for the enhancement of respiratory sounds, IEEE Trans. Biomed. Eng.,vol. 43, no. 4, pp. 421–424, Apr. 1996.

16. Boll, S. F.(1979). Suppression of Acoustic noise in speech using spectral subtraction , IEEE Trans. Acoust., Speech Signal Process., vol. 27, no. 2,pp. 113–120.

17. Moody, G.B., Mark, R.G., Bump, M.A.,.Weinstein, J.S.,.Berman,A.D., Mietus, J.E., & Goldberger, A.L. (1986). Clinical validation of the ECG derived respiration Technique, *Computers in Cardiology, 13,* 507-510.

18. Mared, L., Cline, C., Erhardt, L., Berg, S., & Midgren, B. (2004). Cheyne-Stokes respiration in patients hospitalised for heart failure, [Clinical Trial Research Support, Non-U.S. Gov't]. *Respir Res, 5*, 14. doi: 10.1186/1465-9921-5-14.

19. Smeaton, A.F., & Diamond. D. (2008).Aggregating Multiple Body Sensors for Analysis in Sports, *pHealth*.

20. Womack, B.F. (1971). The Analysis of Respiratory Sinus Arrhythmia Using Spectral Analysis and Digital Filtering, Biomedical Engineering, IEEE Transactions on, 1971. **BME-18**(6): p. 399-409.

21. Sobron, A., Romero, I., & Lopetegi, T. (2010). Evaluation of Methods for Estimation of Respiratory Frequency from the ECG., *Computers in Cardiology, 37,* 513-516

22. O'Brien, C., & Heneghan, C. (2007). A comparison of algorithms for estimation of a respiratory signal from the surface electrocardiogram. [Comparative Study]. *Comput Biol Med, 37*(3), 305-314. doi: 10.1016/j.compbiomed.2006.02.002

23. Lipsitz, L., Hashimoto, F., Lubowsky, L., Mietus, J., Moody, G., Appenzeller, O., & Goldberger, A. (1995). Heart rate and respiratory rhythm dynamics on ascent to high altitude. *Br Heart J, 74*, 390-396.

24. Ding, S., Zhu, X., Chen, W., & Wei, D. (2004). Derivation of Respiratory Signal from Single-Channel ECGs Based on Source Statistics. *International Journal of Bioelectromagnetism, 6*(1).

25. Moody, G.B. (1985)," *Derivation of Respiratory Signals from Multi-lead ECGs".* Computers in Cardiology. **12**: p. 113-116.

26. Travaglini, A., Lamberti, C., DeBie, J., & Ferri, M. (1998). Respiratory Signal Derived from Eight-Lead ECG. *Computers in Cardiology, 25*.

27. Behbehani, K., Vijendra, S., Burk, J. R., & Lucas, E. A. (2002). An Investigation of The Mean Electrical Axis Angle and Respiration During Sleep. *IEEE*

28. Cysarz, D., Zerm, R., Bettermann, H., Fruhwirth, M., Moser, M., & Kroz, M. (2008). Comparison of respiratory rates derived from heart rate variability, ECG amplitude, and nasal/oral airflow [Research Support, Non-U.S. Gov't]. *Ann Biomed Eng, 36*(12), 2085-2094.

29. Langley, P., E.J. Bowers, and A. Murray (2010), Principal Component Analysis as a Tool for Analyzing Beat-to-Beat Changes in ECG Features: Application to ECG-Derived Respiration, Biomedical Engineering, IEEE Transactions on, 2010. **57**(4): p. 821-829.

30. Widjaja, D., Dorado, A. C., Perez, J.C. & Huffel, S. V. (2011). An Improved ECG-Derived Respiration Method using Kernel Principal Component Analysis. *Computers in Cardiology, 38*.

31. Leanderson, S., Laguna, P., & Sörnmo, L. (2003). Estimation of the respiratory frequency using spatial information in the VCG. *Medical Engineering & Physics, 25*(6), 501-507. doi: 10.1016/s1350-4533(03)00017-1

32. Mazzanti, B., Lamberti, C., & Bie, J. d. (2003). Validation of an ECG-Derived Respiration Monitoring Method. *Computers in Cardiology, 30*, 613-616.

33. Bailon, R., Sornmo, L., & Laguna, P. (2006). A Robust Method for ECG-Based Estimation Of the Respiratory Frequency During Stress Testing. *IEEE, 53*(7).

34. Arunachalam, S.P. & L.F. Brown (2009). Real-time estimation of the ECG-derived respiration (EDR) signal using a new algorithm for baseline wander noise removal, in Engineering in Medicine and Biology Society, 2009. EMBC 2009. Annual International Conference of the IEEE. 2009.

35. Park, S.,.(2008). An improved algorithm for respiration signal extraction from electrocardiogram measured by conductive textile electrodes using instantaneous frequency estimation, 147-158, Medical and Biological Engineering and Computing**46**(2): .

36. Kim, J., (2006). Two Algorithms for Detecting Respiratory Rate from ECG Signal", World Congress on Medical Physics and Biomedical Engineering, R. Magjarevic and J.H. Nagel, Editors. Springer Berlin Heidelberg. p. 4069-4071.

37. Babaeizadeh, S., (2011) Electrocardiogram-derived respiration in screening of sleep-disordered breathing, Journal of Electrocardiology, 2011. **44**(6): p. 700-706.

38. Maier, C. & Dickhaus,H. (2010). Central Sleep Apnea Detection from ECG-derived Respiratory Signals, Application of Multivariate Recurrence Plot Analysis. Methods of Information in Medicine,. **49**(5 2010): p. 462-466.

39. Sheila R. Messer, J. A.,& Abbott.D. (2001). Optimal wavelet denoising for phonocardiograms, Microelectronics, 32.

40. Hedayioglu. F. (2009).Heart Sound Segmentation for Digital Stethoscope Integration (Master's thesis, University of Porto). Retrieved from http://repositorio-aberto.up.pt/bitstream/10216/22169/4/MasterThesis.pdf

41. Miwa, H., & Sakai, K. (2009). Development of heart rate and respiration rate measurement system using body-sound. Paper presented at the 9th International Conference on Information Technology and Applications in Biomedicine, Cyprus.

42. M.J. Banet (2009). US Patent No.: USPTO 7481772

43. Pressler, G.A.; Mansfield, J.P., Pasterkamp, H., & Wodicka, G.R. (2004) Detection of respiratory sounds at the external ear, *Biomedical Engineering, IEEE Transactions on* , vol.51, no.12,pp.2089-2096,Dec.2004

44. Tinkelman, D. G., Lutz, C., & Conner, B. (1991). Analysis of breath sounds in normal and asthmatic children and adults using computer digitized airway phonopneumography (CDAP). *Respiratory Medicine, 85*(2).

45. Noma, H. (2005). Wearable Data Acquisition for Heartbeat and Respiratory Information using NAM(Non-Audible Murmur) Microphone Paper presented at the Ninth IEEE International Symposium on Wearable Computers (ISWC'05)

46. Al-Khalidi, F. Q., Saatchi, R., Burke, D., Elphick, H., & Tan, S. (2011). Respiration rate monitoring methods: a review. [Research Support, Non-U.S. Govt Review]. *Pediatr Pulmonol, 46*(6), 523-529. doi: 10.1002/ppul.21416

47. Hult,P., Fjallbrant, T. , Dahle, S., Danielsson, P.& Ask, P.(2000). A method for respiration monitoring by the use of a bioacoustic signal, in Proc 1st Int. Conf. Adv. Med. Signal Inf. Process., Bristol, U.K., 2000 pp.22-25.

48. Werthammer J (1983) Apnea monitoring by acoustic detection of airflow.

49. Corbishley P, C., & E, R.-V. (2008). Breathing detection towards a miniaturized, wearable, battery operated monitoring system. *IEEE*

50. Kaniusas, E., & Helmut. P. (2005).Acoustical signal properties for cardiac/respiratory activity and apneas. IEEE Transactions on BioMedical Engineering, vol 52, no.11, pp.1812-1822.

51. Yongji.F.,Deepak.A., Nhedti.C.(2009).Pulmonary Disease Management System with Distributed Wearable Sensors. 31st Annual International Conference of the IEEE EMBS

52. Malarvili, M., Kamarulafizam, I., Hussain, S., & Helmi, D. (2003). Heart Sound Segmentation Algorithm on Instantaneous Energy of Electrocardiogram. *Computers in Cardiology, 30*, 327-330.

53. Stark, H., & Woods, J. W. (2009). *Probability and Random Processes with Applications to Signal Processing*: Pearson Education

54. What is Sleep Apnea, National Heart Lung and Blood Institute. Retrieved from

http://www.nhlbi.nih.gov/health/health-topics/topics/sleepapnea/

55. Qureshi, A., & Ballard, R. (2003). Obstructive sleep apnea. *J Allergy Clin Immunol, 112*(5). doi: 10.1016/j.jaci.2003.08.031 10.1067/mai.2003.1813

56. Breathing, E., & In, D. (1999). Sleep-related breathing disorders in adults: recommendations for syndrome definition and measurement techniques in clinical research. The Report of an American Academy of Sleep Medicine Task Force. *Sleep (Rochester)* (Vol. 22, pp. 667-689). American Academy of Sleep Medicine. Retrieved from http://www.ncbi.nlm.nih.gov/pubmed/10450601

57. . Sleep Apnea Linked to increased risk of death, National Heart Lung and Blood Institute. Retrieved from http://www.nhlbi.nih.gov/news/press-releases/2008/nhlbi-media-availability-sleep-apnea-linked-to-increased-risk-of-death.html

58. Sleep Apnea Statistics, Retrieved from http://www.sleepapnea-solutions.com/sleep-apnea-statistics.html

59. National commission on sleep disorders Research report. Vol 1. Executive summary and executive report. National Institute of Health,1993:45

60. Polysomnography, Retrieved from http://www.nlm.nih.gov/medlineplus/ency/article/003932.htm

61. Physio-Net, http://physionet.org/cgi-bin/atm/ATM

62. SAS Enterprise Miner help, SAS. Inc.

63. Marwan, N., Carmen Romano, M., Thiel, M., & Kurths, J. (2007). Recurrence plots for the analysis of complex systems. *Physics Reports, 438*(5-6), 237-329. doi: 10.1016/j.physrep.2006.11.001

64. Brin, M., & Stuck, G. (2004). *Introduction to Dynamical Systems*: Cambridge University Press.

65. Webber CL Jr & Zbilut JP (2004). Recurrence quantification analysis of nonlinear dynamical systems. To appear in: Riley MA, Van Orden G (eds) Tutorials in contemporary nonlinear methods for the behavioral sciences.

66. Eckmann, J. P., Kamphorst, S. O., & Ruelle, D. (1987). Recurrence Plots of dynamical systems. *Europhysics Letters, 4*, 973-977.

67. C. Po-Jui. Microfabricated Implantable Parylene-Based Wireless Passive Intraocular Pressure Sensors, *Microelectromechanical Systems, Journal of,* vol. 17, pp. 1342-1351, 2008

68. DeHennis, A. D. & Wise, K. D. (2005). A wireless microsystem for the remote sensing of pressure, temperature, and relative humidity," *Microelectromechanical Systems, Journal of,* vol. 14, pp. 12-22, 2005.

69. Z. Yafan (2001). An ultra-sensitive, high-vacuum absolute capacitive pressure sensor, in *Micro Electro Mechanical Systems, 2001. MEMS 2001. The 14th IEEE International Conference on*, 2001, pp. 166-169.

.

APPENDICES

1. Predictive Modeling XML in SAS Enterprise Miner

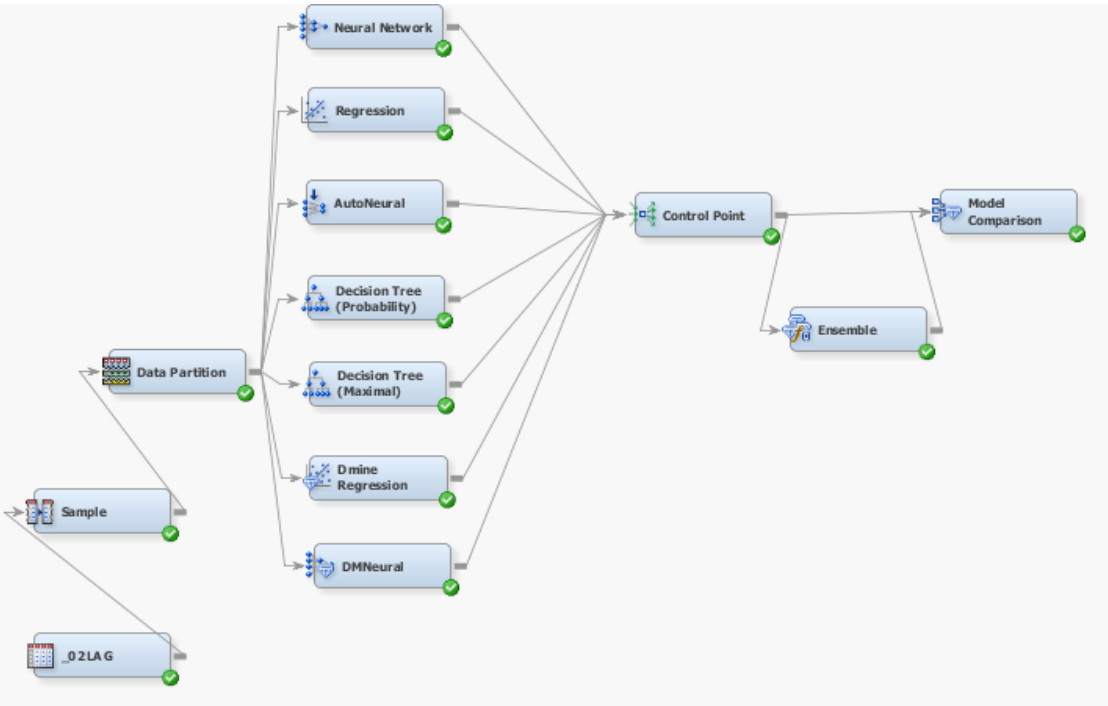

2. Model results

Selected Model	Predecessor Node	Model Node	Model Description	Target Variable	Valid: Misclassification Rate	Valid: Lift
/	AutoNeural	AutoNeural	AutoNeural	Target	0.109198	1.97764
	Ensmbl	Ensmbl	Ensemble	Target	0.115858	1.924838
	Neural	Neural	Neural Net...	Target	0.140777	1.831237
	Tree	Tree	Decision Tr...	Target	0.145737	1.865662
	Tree2	Tree2	Decision Tr...	Target	0.145737	1.865662
	DmineReg	DmineReg	Dmine Reg...	Target	0.170737	1.881638
	DMNeural	DMNeural	DMNeural	Target	0.246595	1.736399
	Reg	Reg	Regression	Target	0.285674	1.778436

3. Principal Components

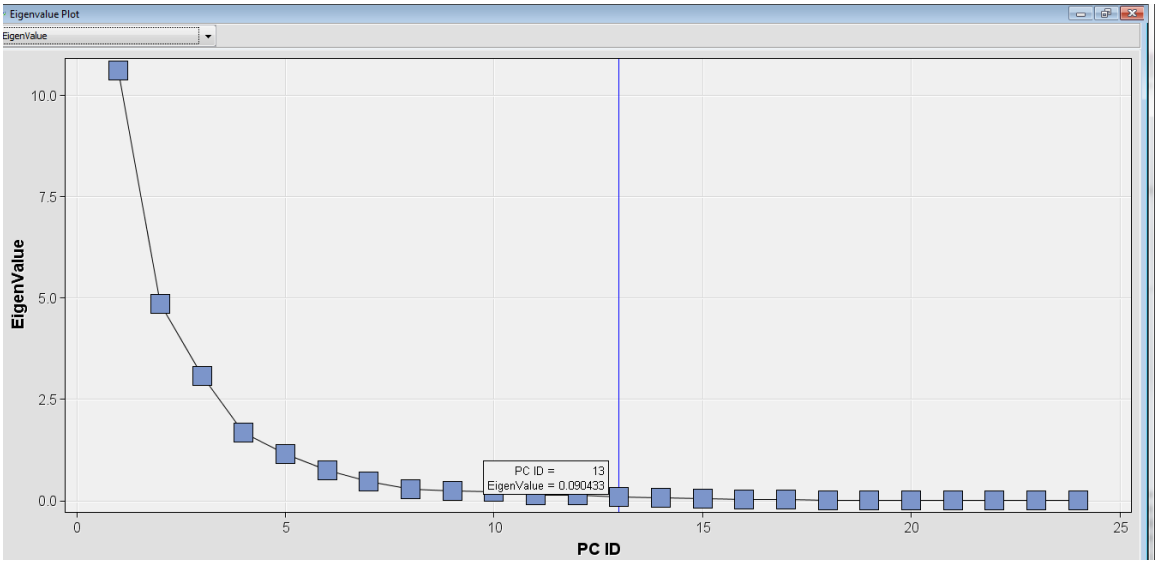

4. Output features obtained using RQA:

```
Output:
Y(:, 1) = RR      (recurrence rate)
Y(:, 2) = DET     (determinism)
Y(:, 3) = <L>     (mean diagonal line length)
Y(:, 4) = Lmax    (maximal diagonal line length)
Y(:, 5) = ENTR    (entropy of the diagonal line lengths)
Y(:, 6) = LAM     (laminarity)
Y(:, 7) = TT      (trapping time)
Y(:, 8) = Vmax    (maximal vertical line length)
Y(:, 9) = T1      (recurrence time of 1st type)
Y(:,10) = T2      (recurrence time of 2nd type)
Y(:,11) = RTE     (recurrence time entropy, i.e., RPDE)
Y(:,12) = Clust   (clustering coefficient)
Y(:,13) = Trans   (transitivity)
```

5. Neural Network Settings:

General	
Node ID	Neural
Imported Data	
Exported Data	
Notes	
Train	
Variables	
Continue Training	No
Network	
Optimization	
Initialization Seed	12345
Model Selection Criterion	Misclassification
Suppress Output	No
Score	
Hidden Units	No
Residuals	Yes
Standardization	No

6. Decision Tree Settings:

Subtree	
Method	Largest
Number of Leaves	1
Assessment Measure	Misclassification
Assessment Fraction	0.25
Cross Validation	
Perform Cross Validation	No
Number of Subsets	10
Number of Repeats	1
Seed	12345
Observation Based Impor	
Observation Based Impor	No
Number Single Var Import	5
P-Value Adjustment	
Bonferroni Adjustment	Yes
Time of Kass Adjustment	Before
Inputs	No
Number of Inputs	1

7. Logistic regression settings:

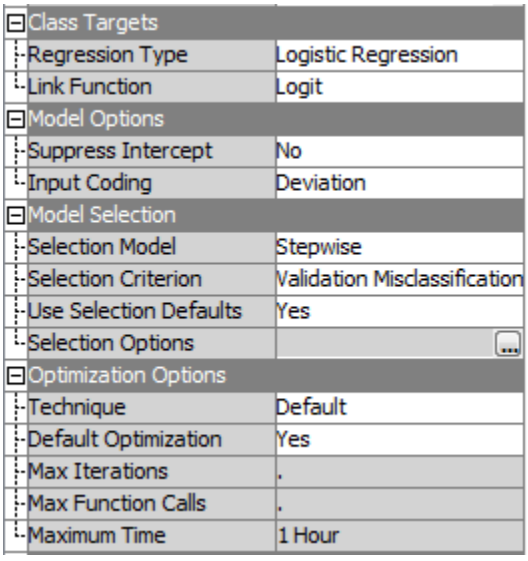

Class Targets	
Regression Type	Logistic Regression
Link Function	Logit
Model Options	
Suppress Intercept	No
Input Coding	Deviation
Model Selection	
Selection Model	Stepwise
Selection Criterion	Validation Misclassification
Use Selection Defaults	Yes
Selection Options	...
Optimization Options	
Technique	Default
Default Optimization	Yes
Max Iterations	.
Max Function Calls	.
Maximum Time	1 Hour

8. AutoNeural node: Default setting

9. Ensemble node settings: Default

VITA

Kunal Karandikar

Candidate for the Degree of

Master of Science

Thesis: ESTIMATION OF SURROGATE RESPIRATION AND DETECTION OF SLEEP APNEA EVENTS FROM DYNAMIC DATA MINING OF MULTIPLE CARDIORESPIRATORY SENSORS

Major Field: Industrial Engineering and Management

Biographical:

Education:

Completed the requirements for the Master of Science in Industrial Engineering and Management at Oklahoma State University, Stillwater, Oklahoma in July, 2012.

Completed the requirements for the Bachelor of Engineering in Electronics Engineering at University of Pune, Pune, India in June, 2009.

Experience:

July 2009- May 2010 Graduate Engineer Trainee, Amara Raja Electronics Limited, New Delhi, India

May 2011-June 2011 Engineering Intern, General Motors India Ltd., Talegaon (Pune), India

Professional Memberships:
Institute of Industrial Engineers
INFORMS
Alpha-Pi-Mu Honor Society

Name: Kunal Karandikar Date of Degree: July, 2012

Institution: Oklahoma State University Location: Stillwater, Oklahoma

Title of Study: ESTIMATION OF SURROGATE RESPIRATION AND DETECTION OF SLEEP APNEA EVENTS FROM DYNAMIC DATA MINING OF MULTIPLE CARDIORESPIRATORY SENSORS

Pages in Study: 82 Candidate for the Degree of Master of Science

Major Field: Industrial Engineering and Management

Scope and Method of Study: This research investigates an approach to derive respiration waveform from heart sound signals, and compare the waveform signal obtained thus with those obtained from alternative methods for deriving respiration waveforms from measured ECG signals. The investigations indicate that HSR can lead to a cost effective alternative to the use of respiratory vests to analyze cardiorespiratory dynamics for clinical diagnostics and wellness assessments. The derived respiratory rate was further used to classify Type III sleep apnea periods using recurrence analysis. Detection of patterns causing sleep apnea could open up opportunities to researchers to better understand and predict symptoms leading to disorders linked with sleep apnea like hypertension, sudden infant death syndrome, high blood pressure and a risk of heart attack.

Findings and Conclusions:

Surrogate respiratory signals derived from heart sounds (HSR) are found to have 32% and 36% correlation with the actual respiratory signals recorded at upright and supine positions, respectively, as compared to EMD derived respiration signals (EDR) that have (18% and 26%) correlation with the respiration waveforms measured in upright and supine positions, respectively. Wavelet-derived respiration (WDR) signals show a higher wave-to-wave correlation (55% and 55%) than HSR and EDR waveforms, but the respiratory sinus arrhythmia (RSA), zero crossing intervals, and respiratory rates of the HSR correlate better with the measured values, compared with those from EDR and WDR signals. Three models were implemented using recurrence analysis to classify sleep apnea events and were compared with a vectorized time series derived model. Advanced predictive modeling tools like decision trees, neural networks and regression models were used to classify sleep apnea events form non-apneic events. Model comparison within preliminary analysis model consisting of nasal respiration as well as its time lagged components and heart rate when compared with recurrence models shows that the preliminary analysis model(vectorized time series) has a lower misclassification rate (10%) than the recurrence models(Model 1: 20% Model 2: 14%, Model 3: 12%).

ADVISER'S APPROVAL: Dr. Satish Bukkapatnam